

# Water Resources Research

## RESEARCH ARTICLE

10.1029/2023WR036421

## A Runoff-On-Grid Approach to Embed Hydrological Processes in Shallow Water Models



### Key Points:

- The Runoff-On-Grid approach integrates subsurface hydrological processes, antecedent soil moisture and soil physics in shallow water models
- The Runoff-On-Grid approach expands the capabilities of the Rain-On-Grid approach introducing non-negligible runoff generation sources
- The DREAM-Iber model supported by enabling technologies provides a high-fidelity reconstruction of the 2020 Esaro flood

### Correspondence to:

P. Perrini,  
[pasquale.perrini@uniba.it](mailto:pasquale.perrini@uniba.it)

### Citation:

Perrini, P., Cea, L., Chiaravallotti, F., Gabriele, S., Manfreda, S., Fiorentino, M., et al. (2024). A runoff-on-grid approach to embed hydrological processes in shallow water models. *Water Resources Research*, 60, e2023WR036421. <https://doi.org/10.1029/2023WR036421>

Received 16 OCT 2023

Accepted 11 JUN 2024

### Author Contributions:

**Conceptualization:** Pasquale Perrini, Luis Cea, Salvatore Manfreda, Mauro Fiorentino, Andrea Gioia, Vito Iacobellis

**Data curation:** Pasquale Perrini, Francesco Chiaravallotti, Salvatore Gabriele

**Formal analysis:** Pasquale Perrini

**Investigation:** Pasquale Perrini, Luis Cea, Francesco Chiaravallotti, Salvatore Gabriele, Salvatore Manfreda, Mauro Fiorentino, Andrea Gioia, Vito Iacobellis

**Methodology:** Pasquale Perrini, Luis Cea, Salvatore Manfreda, Mauro Fiorentino, Andrea Gioia, Vito Iacobellis





**Supervision:** Luis Cea, Andrea Gioia, Vito Iacobellis

**Validation:** Pasquale Perrini, Luis Cea, Salvatore Manfreda, Mauro Fiorentino, Andrea Gioia, Vito Iacobellis

**Writing – original draft:** Pasquale Perrini

© 2024. The Authors.

This is an open access article under the terms of the [Creative Commons Attribution License](https://creativecommons.org/licenses/by/4.0/), which permits use, distribution and reproduction in any medium, provided the original work is properly cited.

Pasquale Perrini<sup>1,2,3</sup> , Luis Cea<sup>2</sup> , Francesco Chiaravallotti<sup>4</sup> , Salvatore Gabriele<sup>4</sup>, Salvatore Manfreda<sup>5</sup> , Mauro Fiorentino<sup>6</sup>, Andrea Gioia<sup>3</sup>, and Vito Iacobellis<sup>3</sup>

<sup>1</sup>Department of Soil, Plant and Food Science, University of Bari Aldo Moro, Bari, Italy, <sup>2</sup>Water and Environmental Engineering Group, Center for Technological Innovation in Construction and Civil Engineering (CITEEC), University of A Coruña, A Coruña, Spain, <sup>3</sup>Department of Civil, Environmental, Land, Building Engineering and Chemistry, Polytechnic University of Bari, Bari, Italy, <sup>4</sup>Research Institute for Geo-Hydrological Protection, National Research Council, Rende, Italy, <sup>5</sup>Department of Civil, Building and Environmental Engineering, University of Naples Federico II, Naples, Italy, <sup>6</sup>Department of European and Mediterranean Cultures: Architecture, Environment and Cultural Heritage, University of Basilicata, Matera, Italy

**Abstract** Catchment-scale hydrological models encountered dichotomies with the numerical hydrodynamic models when describing surface routing process. We propose a new modeling framework, the so-called “Runoff-On-Grid” approach, for embedding distributed process-based hydrological modeling into shallow water models, as an alternative to the traditional Fully Hydrodynamic Approach (also known as Rain-On-Grid). Antecedent Soil Moisture, subsurface dynamics, and other topsoil hydrological processes are implicitly integrated in the governing hydrodynamic equations via the proposed methodology. The resulting hydrological-hydrodynamic coupling, based on the DREAM distributed hydrological model and the Iber+ shallow water model, enhances the capabilities of both reference models. Through introducing non-negligible runoff generation sources, the Runoff-On-Grid approach extends the surface hydrodynamic modeling to medium-sized vegetated and/or (semi)humid catchments, bypassing the limitations of the widespread hydrological losses' empirical formulations. Employed in an event-based analysis within a High-Performance Computing framework, the DREAM-Iber model provides an efficient and reliable reconstruction of the November 2020 flood that occurred in Crotona (Italy), envisaging consequences of similar future scenarios. We show that the proposed modeling technique, nested within emerging environmental technologies and robust on-site data, details the flood hazard inducing processes merging physical hydrology with advanced hydrodynamics.

**Plain Language Summary** In this scientific contribution, the potential of combining two different operational tools, namely distributed rainfall-runoff and flood models, is investigated. An hindcast procedure has been used as reference to assess both the hydrological processes and the inundations at the catchment-scale. In this context, were exploited cutting edge computational and environmental technologies, which significantly quickened the simulations and enabled a high-fidelity reconstruction of the extreme meteorological event. According to our findings, there is merit of the proposed approach for bridging the dichotomies between the hydrological and hydrodynamic simulators. This can favor of a more comprehensive method to reduce the limitation of the standalone models.

## 1. Introduction

As climate change gives rise to an increasing number of worrying meteorological events, there is a growing need for heuristic approaches to the modeling of extreme events such as floods. Bridging the dichotomies that exist between the various differing perspectives on this issue remains a significant challenge (Blair et al., 2019; Savenije, 2009). However, it is also a great opportunity to enhance both the understanding of disaster-inducing processes and process-based hydrological models (K. Beven, 2007; Kastens et al., 2009). The surface, subsurface, and profound hydrological processes have always suffered a conceptual dichotomy, as noted in literature (Staudinger et al., 2019). Although we know the various physical processes that control rainfall-runoff transformation (McMillan, 2022), the generalized mathematical description of some of these encounter a variety of epistemic uncertainties (K. J. Beven & Alcock, 2012; Blöschl et al., 2019; Merz & Thielen, 2005; Nearing et al., 2016; Tartakovsky, 2007). Nonetheless, there has been notable progress in our understanding of the

**Writing – review & editing:** Luis Cea, Francesco Chiaravalloti, Salvatore Gabriele, Salvatore Manfreda, Mauro Fiorentino, Andrea Gioia, Vito Iacobellis

fundamental processes, due to the increasing use of innovative modeling techniques and the comparison and assessment of different codes (Clark et al., 2015; Fenicia et al., 2008, 2014, 2016). In catchment hydrology, models are commonly based on the mass, momentum and energy conservation principles applied to the water flow above and below the surface of the earth. At the state of the art, it is not possible to rank the models in order of performance, in that the complexity of the structure of models cannot be directly related to the quality of results (e.g., Orth et al., 2015; Perrin et al., 2001; van Esse et al., 2013). Nonetheless, the physically-based simulators of reference are the Integrated Surface-Subsurface Hydrological Models (ISSHM) (Paniconi & Putti, 2015). These are based on the numerical solution of the system formed by the three-dimensional Richards equation for modeling subsurface and profound flows in porous media and a simplified form of the mass and momentum conservation laws for modeling overland flow (OF). Considering the high degree of complexity in coupling several concatenated processes and interactions at different temporal and spatial scales (Blöschl, 2022; McDonnell et al., 2007), the implementation of these comprehensive ISSHM in realistic study cases is still not widely applicable. At the catchment scale, the variability in parameters and state variables, poorly known boundary and initial conditions, as well as the complexity of the unsaturated zone, lead to a high predictive uncertainty. This situation continues to favor simplified assumptions in describing large scale processes through perceptual (i.e., conceptual) models (K. J. Beven & Chappell, 2021; Fenicia & McDonnell, 2022; Savenije, 2010; Sivapalan, 2003).

An alternative approach, which has garnered increasing interest, is Rain-on-Grid modeling (Hall, 2015), sometimes referred to as the Fully Hydrodynamic Approach (FHA) or the Direct Rainfall method. Here, the surface processes are modeled with the full system of 2D shallow water equations (2D-SWE), while the subsurface processes are forcibly simplified by the adoption of empirical loss methods. The FHA enables, across the entire computational mesh, a holistic and physically based representation of the surface runoff based on the 2D-SWE. This methodology is particularly well-suited to pluvial or flash floods in small and urbanized catchments with relatively steep slopes and poorly permeable soils. Under these conditions the basin response to the rainfall input, as well as the surface runoff generation and routing, are of most importance (Costabile et al., 2013; Godara et al., 2023). The methodology is justified in such instances, where the influence of subsurface flow on event-based flood hydrographs is minimal, with infiltration-excess (or hortonian) OF assuming a dominant role (Rehman et al., 2003). Under these conditions it is deemed appropriate to rely solely on a simplified methodology to estimate net rainfall. The widespread success of this approach in flood hazard assessment can be credited to recent advances in High Performance Computing (HPC) techniques using Graphics Processing Units (GPU), and to the availability of high-resolution topographic data. In recent years, the FHA has been tested for urban drainage modeling (Buttinger-Kreuzhuber et al., 2022; Cea, Garrido, Puertas, et al., 2010; Montalvo et al., 2024; Sañudo et al., 2024), flood hazard modeling at regional and continental scale (Bates et al., 2021; Cea et al., 2022, 2024; Fraga et al., 2019; Lacasta et al., 2015; Xia et al., 2019), real-time flood forecasting (Ming et al., 2020), soil erosion modeling at the catchment scale (Costabile et al., 2024; Uber et al., 2021), rainwater harvesting techniques (Tamagnone, Cea, et al., 2020; Tamagnone, Comino, & Rosso, 2020), and hydro-morphological characterization of basins and streams (Barbero et al., 2022; Costabile & Costanzo, 2021; Costabile et al., 2019).

However, there are still some limitations in the application of the FHA at the catchment scale. These stem from the simplified way in which subsurface processes and soil physics are in general incorporated in the 2D-SWE. In most of the above applications of the FHA, infiltration losses are modeled using empirical event-based formulations. While topsoil wetness (i.e., root zone for hydrological applications) is rarely assessed explicitly through water budget equations, despite it being a key element that controls a number of hydrological processes (Massari et al., 2014; Nied et al., 2017). This reduces the performance of the FHA when applied to long storm events with several rainfall peaks, where the time evolution of soil infiltration does not follow the exponential trend given by the empirical formulations. For the same reason, it hinders the initialization or warm-up of the model in the days prior to the storm event. Moreover, exfiltration is generally not taken into consideration in the FHA, and thus all the water infiltrated into the soil cannot return to the surface in other parts of the basin. Hence, to extend the use of the FHA to catchment hydrological modeling, a more thorough assessment of soil conditions and dynamics, including surface-subsurface interactions and flows, is needed.

This paper proposes a new approach, called Runoff-On-Grid, for embedding distributed topsoil hydrological processes in 2D shallow water models, using the DREAM model (Manfreda et al., 2005) and the Iber model

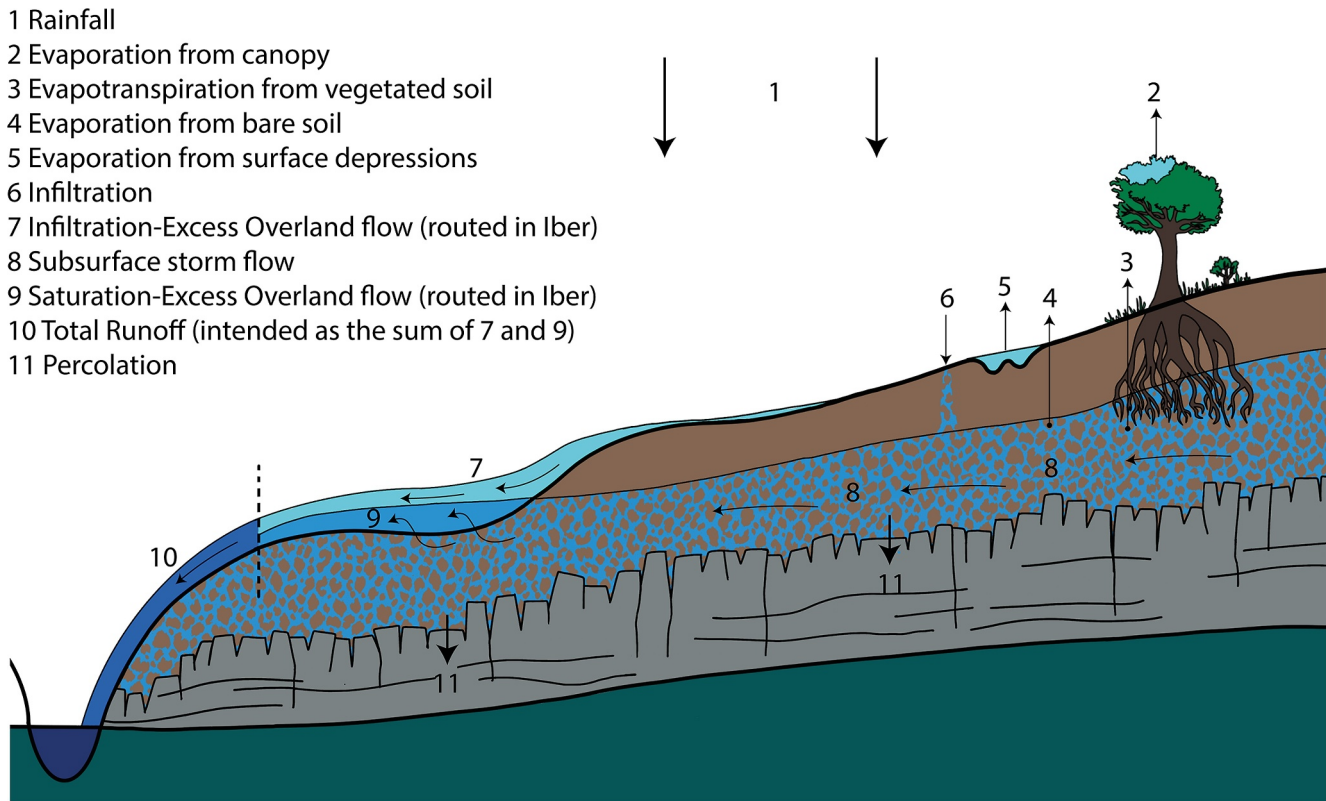


**Figure 1.** Schematic representation of the hydrological processes simulated in the DREAM-Iber Runoff-On-Grid application.

(Bladé et al., 2014) as references for the proposal. The innovative approach here, supported by multiple enabling technologies (Rigon et al., 2022) (i.e., emerging geospatial technologies, HPC, Virtual reality visualization) and unconventional on-site data (i.e., photos, videos, newspaper information), has been tested in the reconstruction of a recent historical flood event in Crotona (South Italy). The good model performance obtained, encourages the implementation of the method in other case studies.

## 2. Materials and Methods

### 2.1. Runoff-On-Grid Approach

The FHA might not fully or adequately represent the relevant hydrological processes in medium and large catchments or in wet and vegetated areas. Physical properties of the topsoil and antecedent soil moisture (ASM) conditions can significantly attenuate (or amplify) the effects of storm events, triggering surface-subsurface interactions such as the generation of saturation-excess OF (Dunne & Leopold, 1978; Freeze, 1974). From a conceptual point of view, the primary constraint of simplified loss methods used in hydrology is their inability to assess explicitly the availability of soil water, which can have a significant effect on multiple subsurface processes (e.g., K. Beven & Germann, 2013; McDonnell, 1990; Weiler et al., 2006).

The Runoff-On-Grid approach described in the current paper combines surface and subsurface dynamics with the shallow water equations through a conceptual representation of subsurface water fluxes. The methodology relies on a distributed process-based hydrological model to produce a total runoff depth variable in time and space across the whole catchment, preserving an accurate routing of surface runoff based on the application of the 2D-SWE at the catchment scale. For the sake of clarity, in this context “total runoff” refers to the combined contribution of various sources representing the net volumes of runoff that contribute to flood generation. The hydrological model employed on the Runoff-On-Grid approach is based on the DREAM model. This has undergone testing and validation in various research encompassing multiple objectives (Fiorentino et al., 2007; Gigante et al., 2009; Iacobellis et al., 2013; Manfreda et al., 2011; Milella et al., 2012). The shallow water model

used is Iber, which has already been validated for OF applications in several studies (Cea & Bladé, 2015; Cea et al., 2014, 2022, 2024; Cea, Garrido, & Puertas, 2010). The roles of the two models are complementary, but conceptually different. The DREAM model simulates the surface water balance by calculating soil water content at the catchment scale and various sources of runoff volume. Meanwhile, the Iber model route the total runoff volumes on the ground surface and quantifies the magnitude of flooding in terms of hydrodynamic variables. A schematic hillslope representation of the processes simulated in the DREAM-Iber coupled model, is shown in Figure 1.

## 2.2. Distributed Hydrological Model

The DREAM (Distributed model for Runoff, Evapotranspiration, and Antecedent soil Moisture) model (Manfreda et al., 2005) is realized in a raster-based uniform grid discretization framework that explicitly considers the spatial heterogeneity of the basin using data contained in digital elevation models, land use maps, soil texture maps, soil hydraulic properties and vegetation parameters. Physically-based conceptual relationships are used to simulate the dynamics of hydrological processes, ensuring a feasible representation of all the relevant processes that can contribute within a short time-lapse to a flood event. The range of application of the current version of the model encompasses small to medium-sized catchments in both urban and rural landscapes. The model includes two sub-modules operating at different time scales that can also be applied separately. The *Daily* module (hereafter the warm-up module) is designed to reproduce daily soil dynamics and provide ASM conditions for the *Sub-Hourly* module (hereafter the *runoff* module), which aims to reproduce the total runoff generation across the whole catchment. In order to model the basin's response to intense rainfall, a time step of 15 min may be necessary in the *runoff* module to capture the variations of the total runoff budget more precisely. Going further and using a time step of the order of seconds is usually not significant, and can lead to spurious results that do not represent the correct hydrological behavior of the catchment. The present version of DREAM has been updated through the introduction of new formulations for computing surface runoff generation, rainfall interception, surface depression storage and actual evapotranspiration. In addition, through the Runoff-On-Grid approach, it exploits the 2D-SWEs for surface runoff routing (replacing the one-dimensional steady flow-time response function used in its original formulation), which is the most notable innovation of the coupled methodology presented here. In particular, the output of the DREAM model is intended to be the spatial distribution of total surface runoff for each computational time step, which is used as an input (i.e., source term) in the Iber model. Of note, in the present version of the model only surface runoff generated by infiltration-excess and/or saturation-excess, arising from the combination of surface and subsurface processes, was considered to compute the total surface runoff, while the contribution of the baseflow for this application was not taken into account.

### 2.2.1. Soil Water Budget and Total Runoff Budget

The DREAM model schematizes the soil as a uniform bucket with limited capacity (Manabe, 1969) corresponding to the soil water capacity. The soil water content is evaluated as the product of the volumetric soil moisture content ( $\theta$  [-]) and the soil rooting depth ( $D$  [mm]). The reference wetness contents at the field capacity ( $S_c$ ), at the wilting point ( $S_{wp}$ ), at saturation ( $S_{max}$ ), and the saturated hydraulic conductivity ( $K_s$ ), are estimated through the pedo-transfer-function proposed by Saxton and Rawls (2006), while the residual water content ( $S_r$ ) is computed following Rawls et al. (1982). Accounting for several distributed vertical fluxes and for the local effect of sub-surface lateral flow (sub-horizontal flux), the DREAM model establishes, for every computational cell and for each time step, two different budget equations, these applied above and below the ground level. The first refers to the soil water content at the instant of time  $t + \Delta t$ , and it can be expressed as:

$$S_{t+\Delta t} = \min(S_t + I_t - ET_{soil,t} - RG_t + RS_t, S_{max}) \quad (1)$$

while the second refers to the total runoff cumulated during the time step  $\Delta t$  ( $R_{tot,t+\Delta t}$ ):

$$R_{tot,t+\Delta t} = \max(0, P_{gross,t} - \Delta W_{int,t} - I_t - \Delta W_{dep,t} + SS_t) \quad (2)$$

where  $I_t$  (mm/ $\Delta t$ ) is the water infiltrated into the soil,  $ET_{soil}$  (mm/ $\Delta t$ ) is the evapotranspiration from the soil,  $RG_t$  (mm/ $\Delta t$ ) is the water percolated into the deep soil,  $RS_t$  (mm/ $\Delta t$ ) is the subsurface lateral flow into the computational cell,  $S_{max}$  (mm) is the soil water capacity,  $P_{gross,t}$  (mm/ $\Delta t$ ) is the gross precipitation,  $\Delta W_{int,t}$  (mm/ $\Delta t$ ) is

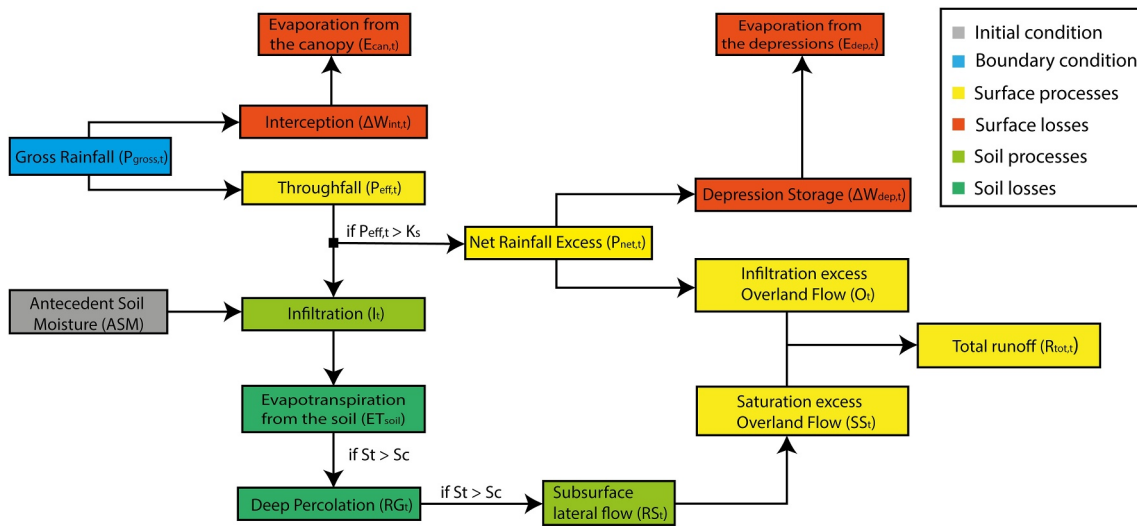


Figure 2. Flowchart for computing “Total Runoff” with the DREAM model.

the water intercepted by the canopy,  $\Delta W_{dep,t}$  (mm/ $\Delta t$ ) is the water stored into the surface depression, and  $SS_t$  (mm/ $\Delta t$ ) is the saturation-excess OF. The components of the model (Figure 2) and related mathematical equations are detailed in the following subsections. The chronological computation follows the order in which the equations are written, which means that, specifically for the soil water contents, the variables are constantly updated after each process computation.

### 2.2.2. Interception

Although interception is usually considered a negligible component when simulating an extreme event, it is important for assessing the whole water balance. It is here modeled as a simple bucket that stores water from the gross precipitation until saturation. The water intercepted by each grid element during a computational time step is modeled following the method proposed by Braden (1985) and Von-Hoyningen-Huene (1983), and can be expressed as:

$$\Delta W_{int,t} = \min \left( W_{int\_max,t} - W_{int,t}, W_{int\_max,t} \left( 1 - \left( 1 + \frac{M_t \cdot P_{gross,t}}{W_{int\_max,t}} \right)^{-1} \right) \right) \quad (3)$$

$$W_{int\_max,t} = a \cdot LAI_t \quad (4)$$

$$M_t = 1 - \exp(-\mu \cdot LAI_t) \quad (5)$$

where  $W_{int\_max,t}$  (mm) is the maximum capacity of interception,  $a$  is an empirical parameter equal to 0.2 (Dickinson, 1984),  $LAI_t$  (–) is the Leaf Area Index,  $M_t$  (–) represents the fraction of soil covered by vegetation (Eagleson, 1982), and  $\mu$  (–) is the light extinction coefficient depending on land use, parametrized by Larcher (1975). The throughfall ( $P_{eff,t}$ ) that arrives at the soil surface is estimated by subtracting the interception component from the gross Precipitation ( $P_{gross,t}$ ).

$$P_{eff,t} = P_{gross,t} - \Delta W_{int,t} \quad (6)$$

### 2.2.3. Infiltration and Net Rainfall Excess

The net rainfall excess is computed as a function of the soil hydraulic characteristics and rainfall intensity, and its activation is modeled using a threshold mechanism. Following Horton's theory (Betson, 1964; Horton, 1933, 1941), the production of surface runoff is assumed to be strictly influenced by the topsoil hydraulic conductivity. This is a common and generalizable factor that orchestrates the direct generation of surface runoff from the top downward. If the throughfall rate is lower than a threshold equal to the saturated hydraulic conductivity ( $K_s$ ), the

surface runoff production is not activated, and the soil continues to fill until saturation. When the threshold is exceeded, the partial-area mechanism of surface runoff production is activated, and the water infiltrated into the soil ( $I_t$ ) is modeled following the formulation adapted from De Smedt et al. (2000):

$$I_t = \min\left(S_{\max} - S_t, P_{\text{eff},t} \cdot \left(1 - C_p \cdot \left(\frac{S_t}{S_{\max}}\right)^\alpha\right)\right) \quad (7)$$

where  $C_p$  (–) is the potential runoff coefficient, parametrized as a function of the terrain slope, USDA soil type and land use following Liu and De Smedt (2004), and  $\alpha$  is a coefficient that reflects the attenuation of the runoff production for very high rainfall intensities (Dunne, 1991), which is considered a case-dependent and site-specific calibration parameter. Consequently, the net rainfall excess ( $P_{\text{net},t}$ ) is computed as:

$$P_{\text{net},t} = P_{\text{eff},t} - I_t \quad (8)$$

#### 2.2.4. Depression Storage and Infiltration-Excess OF

The depression storage occurs only when the net rainfall excess is positive ( $P_{\text{net},t} > 0$ ). Following Linsley et al. (1975) and Viessman et al. (1989), the depth of water held in surface depressions at any given time can be expressed as:

$$\Delta W_{\text{dep},t} = \min\left(W_{\text{dep\_max}} - W_{\text{dep},t}, W_{\text{dep\_max}} \left(1 - \exp\left(-\frac{P_{\text{net},t}}{W_{\text{dep\_max}}}\right)\right)\right) \quad (9)$$

where  $W_{\text{dep\_max}}$  (mm) is the depression storage capacity. The depression storage is assumed to increase with the net precipitation up to an asymptotic value corresponding to  $W_{\text{dep\_max}}$  (mm), which is parametrized as a function of the terrain slope, USDA soil type and land use, following Liu and De Smedt (2004). It should be noted that both surface runoff and depression storage occur simultaneously, allowing some of the water to become OF, even if the net rainfall excess is less than the depression storage capacity. The infiltration-excess OF ( $O_t$ ) is evaluated as the difference between the net rainfall excess  $P_{\text{net},t}$  and the water held in the depressions during the current time step:

$$O_t = P_{\text{net},t} - \Delta W_{\text{dep},t} \quad (10)$$

#### 2.2.5. Actual Evapotranspiration

The actual evapotranspiration is represented in the model by four conceptual components, two for the vegetated fraction of the surface ( $ET_{\text{veg}}, E_{\text{can}}$ ) and two for the remaining bare surface ( $E_{\text{bare}}, E_{\text{dep}}$ ). All the components are computed as a function of potential evapotranspiration ( $EP_t$ ), which must be introduced by the user as input data in the model.

The  $EP_t$  is split by considering the fraction of vegetated soil ( $M_t$ ) for each grid cell, thus:

$$EP_{\text{veg},t} = EP_t \cdot M_t \quad (11)$$

$$EP_{\text{no\_veg},t} = EP_t \cdot (1 - M_t) \quad (12)$$

The actual evapotranspiration from the vegetated surface is computed as direct evaporation from the canopy ( $E_{\text{can},t}$ ), following Deardorff (1978) and Famiglietti and Wood (1994), and evapotranspiration from the vegetated soil ( $ET_{\text{veg},t}$ ):

$$E_{\text{can},t} = \min\left(W_{\text{int},t}, \left(\frac{W_{\text{int},t}}{W_{\text{int\_max},t}}\right)^{\frac{2}{3}} \cdot (EP_{\text{veg},t})\right) \quad (13)$$

$$ET_{\text{veg},t} = \min\left(1, \frac{4}{3} \frac{S_t}{S_{\max}}\right) \cdot (EP_{\text{veg},t} - E_{\text{can},t}) \quad (14)$$

In the surface not covered by vegetation, the actual evaporation is evaluated through a potential rate that depends on the available water in the depressions ( $E_{dep,t}$ ) and the remaining potential evapotranspiration rate from bare soil ( $E_{bare,t}$ ), estimated as in Milella et al. (2012) following the equation proposed from Bonan (1996):

$$E_{dep,t} = \min(W_{dep,t}, EP_{no\_veg,t}) \quad (15)$$

$$E_{bare,t} = \left( \frac{r_a}{r_a + r_s} \right) \cdot (EP_{no\_veg,t} - E_{dep,t}) \quad (16)$$

$$r_a = \frac{1}{\rho C_e \bar{u}} \quad (17)$$

$$r_s = r_a \left( \frac{1 - (S_t - S_r)/(S_{max} - S_r)}{(S_t - S_r)/(S_{max} - S_r)} \right) \quad (18)$$

where  $r_a$  (s/m) is the aerodynamic resistance,  $r_s$  (s/m) is the soil resistance,  $\rho$  is the air density ( $\text{kg/m}^3$ ),  $C_e$  is the bulk coefficient for latent heat transport,  $\bar{u}$  is the mean wind velocity (m/s), and  $S_r$  is the residual water content. The resulting real evapotranspiration from the soil ( $ET_{soil,t}$ ) that contributes to the soil water balance in Equation 1 is the sum of the two components:

$$ET_{soil,t} = E_{bare,t} + ET_{veg,t} \quad (19)$$

### 2.2.6. Percolation

Groundwater recharge occurs as percolation through the vadose zone and is represented as vertical leakage that is released only when the soil moisture content is above the field capacity ( $S_c$ ). Its value is estimated following Eagleson (1978):

$$RG_t = \min \left( S_t - S_c, K_s \cdot \left( \frac{S_t}{S_{max}} \right)^\beta \right) \quad (20)$$

where the parameter  $\beta = (2 + 3m)/m$  represents the pore disconnectedness index estimated through the pore-size distribution index ( $m$ ), following Rawls and Brakensiek (1985).

### 2.2.7. Subsurface Lateral Flow and Saturation-Excess OF

Subsurface lateral flow is evaluated after percolation and becomes significant only when the water content of the root zone takes values between the field capacity and the saturation. This process is assumed to occur at the sub-basin scale, necessitating the division of the catchment into sub-domains in accordance with Horton's stream ordering method. Thereby, each cell of the whole catchment is reassigned to each sub-basin, which represent a standalone system for the computation of subsurface lateral flow. The soil water that locally exceeds the field capacity is redistributed within each sub-catchment of the Horton order immediately smaller than that of the whole basin. The redistribution mechanism implemented in the DREAM model exploits the properties of the Topographic Wetness Index (TWI) introduced by Kirkby (1975). The TWI describes a steady state condition of soil moisture in a catchment that reflects the tendency of water to accumulate in regions with a large drainage area and a relatively low terrain slope. It depends on the drainage area per unit contour length and on the terrain slope in the steepest descent direction (K. J. Beven, 2011). Consequently, during a storm event, the cells with a high TWI may reach saturation rapidly and water exceeding the soil capacity is exfiltrated and contributes to the production of surface runoff. The spatial redistribution in DREAM is introduced for the evaluation of the lateral flow exchange ( $RS_i$ ) in Equation 1. Writing the equation for a generic grid cell  $j$  requires evaluating the volume of lateral flow in any cell  $i$  of the basin, hence for the purpose of the clarity of the conceptual model we here introduce the cell subscript  $j$  ( $RS_{t,j}$ ):

$$RS_{t,j} = \left( \frac{\text{TWI}_j \sum_{i=1}^{N(t)} \max[c(S_{t,i} - S_{c,i}), 0]}{\sum_{i=1}^{N(t)} \text{TWI}_i} \right) - \max[c(S_{t,j} - S_{c,j}), 0] \quad (21)$$

where  $RS_{t,j}$  is the subsurface lateral flow into cell  $j$ ,  $\text{TWI}_i$  is the topographic wetness index of cell  $i$ ,  $N(t)$  is the number of cells in the sub-basin that at the time  $t$  exceed the field capacity, and  $c$  [ $\text{T}^{-1}$ ] is the redistribution coefficient (to be used as a calibration parameter). Note that  $RS_{t,j}$  can be negative depending on the balance between water entering and leaving the cell. The saturation excess OF ( $SS_t$ ) exceeding the soil storage capacity is evaluated for any cell (hence eliminating the subscript  $j$ ) as:

$$SS_t = \max(0, (RS_t + S_t) - S_{\max}) \quad (22)$$

It should be noted that the explicitly distributed estimation of the total runoff embeds a conceptual distinction from the net rainfall generated by the abovementioned empirical loss methods of the FHA. Subsurface runoff is not directly influenced by rainfall, but rather closely linked to the availability of soil water. Hence, this process can lead to local values of total runoff exceeding the gross rainfall in proximity to the stream network, especially during a storm event under highly saturated conditions. Moreover, total runoff values can also occur after a storm event in the absence of precipitation.

### 2.3. Shallow Water Model

The shallow water model used in this study is the freely distributed software Iber+ (García-Feal et al., 2018), which is a recent HPC implementation of the original Iber code (Bladé et al., 2014). The model solves the 2D-SWE by using GPU parallelization techniques, achieving speed-ups of up to two-orders of magnitude with respect to its sequential implementation. In the Runoff-On-Grid approach, the total runoff budget computed with DREAM (Equation 2) is included as a spatiotemporal distributed source term in the 2D mass conservation equation, which can be expressed as:

$$\frac{\partial h}{\partial t} + \frac{\partial q_x}{\partial x} + \frac{\partial q_y}{\partial y} = R_{\text{tot}} \quad (23)$$

where  $(q_x, q_y)$  are the two components of the unit discharge and  $h$  is the water depth. The conservation of momentum in the two horizontal directions is expressed as:

$$\frac{\partial q_x}{\partial t} + \frac{\partial}{\partial x} \left( \frac{q_x^2}{h} + \frac{gh^2}{2} \right) + \frac{\partial}{\partial y} \left( \frac{q_x q_y}{h} \right) = -gh \frac{\partial z_b}{\partial x} - g \frac{n^2}{h^{7/3}} |q| q_x \quad (24)$$

$$\frac{\partial q_y}{\partial t} + \frac{\partial}{\partial y} \left( \frac{q_y^2}{h} + \frac{gh^2}{2} \right) + \frac{\partial}{\partial x} \left( \frac{q_x q_y}{h} \right) = -gh \frac{\partial z_b}{\partial y} - g \frac{n^2}{h^{7/3}} |q| q_y \quad (25)$$

where  $n$  is the Manning roughness coefficient,  $g$  is the gravity acceleration,  $|q|$  is the modulus of the unit discharge and  $z_b$  is the bed elevation. These equations are solved using an explicit unstructured finite volume solver that includes a specific numerical scheme for rainfall-runoff applications, the Decoupled Hydrological Discretization presented in Cea and Bladé (2015). Briefly, this scheme combines the hydrostatic pressure gradient with the bed slope in a single term (function of the free surface gradient). As a result, more stable, efficient, and faster simulations are achieved when modeling rainfall-runoff at the catchment scale. Since the DREAM and the Iber models use a different spatial discretization, the raster-based volumes of total runoff ( $R_{\text{tot}}$ ) computed with DREAM are transferred to the unstructured mesh of Iber using the nearest neighborhood interpolation. All the numerical simulations of Iber+ in the present study were performed on the HPC Cluster of the ReCas infrastructure (Antonacci et al., 2017), equipped with an NVIDIA A100 Tensor Core GPU (40 GB).



### 3. Study Case: The Flood of Crotona in 2020

The proposed methodology was tested in the Esaro catchment, located in Crotona (Calabria Region, Southern Italy), which has already been investigated extensively due to the intense flood damage observed in recent decades (Costabile et al., 2020; Macchione et al., 2019). Covering an area of approximately 110 km<sup>2</sup>, its impulsive nature can be attributed to both its dense drainage network and steep topographic gradients, along with a significant proportion of impervious surfaces. Furthermore, a recent detailed study on the sensitivity to desertification of a significant agricultural area in the province of Crotona (Coscarelli et al., 2016) classified the landscape into “potential fragile and critical areas” (worst class).

Between 21 and 23 November 2020 a severe meteorological event occurred in the region, impacting a significant part of the Ionic coast. In less than 48 hr, around two-thirds of the annual average rainfall (~650 mm/year) was recorded. The post-event report provided by the “Centro Funzionale Multirischi—Agenzia Regionale per la Protezione dell'Ambiente della Calabria” (<https://www.cfd.calabria.it/>; last accessed 29 May 2023) hereinafter CFM-ARPACAL, classified this event using the Two Component Extreme Values distribution (Rossi et al., 1984) as a 171-year return period event, referring to a 24-hr rainfall duration. The intense rainfall provoked important damage in the city center of Crotona and multiple overflows along the concluding part of the ephemeral river (here Esaro river). More than 50 interventions by local authorities to rescue people stuck in cars or at homes with ground or basement floors were reported. Jointly, it is worth to mention that the Esaro River has remained unattended and uncleansed for two decades, fostering the growth of thick, spontaneous reeds (i.e., *Phragmites australis*) spanning meters in height (Figure 3d). For further information, the reader should refer to the specific event report by the National Research Council, Research Institute for Geo-Hydrological Protection, hereinafter CNR-Irpi (available online in Italian at <http://irpics.cnr.it/>; accessed on 20 May 2023), and to the documentary of the Esaro river (available on YouTube, in Italian, <https://www.youtube.com/watch?v=uD24Ieh3NVg&t=118s>, last accessed 22 July 2023).

In this context, we seek to comprehensively hindcast the event at the catchment scale, elucidating the inducing processes and factors that provoked the flooding, exploiting both process-based hydrological modeling and advanced numerical hydrodynamics.

#### 3.1. Data and Workflow

The main driving variables for a reliable reconstruction of an extreme flood event through process-based models are the spatiotemporal distribution of rainfall and the ASM conditions (Nied et al., 2017). A proper estimation of the ASM content can provide a much more robust starting point for the hindcasting (Kim et al., 2018), which was carried out with the DREAM warm-up module. In the first applications of the DREAM model (e.g., Manfreda et al., 2005) very long warm-up periods were implemented (7 years) whose hypothetical initial condition was proved to not affect soil water content at the end of the simulation. In this study we exploited satellite-based soil moisture data, both to avoid the choice of a hypothetical initial condition for the warm-up period and to implicitly reduce its length. The starting date of the warm-up period was chosen in order to have an expected dry soil condition (i.e., below the field capacity), proved by reliable satellite-based information. For the Mediterranean climate patterns of the area under investigation, summer is the season with least expected soil water content. Hence, for the purpose of this paper (i.e., the simulation of the November 2020 event) the DREAM model encompassed a warm-up period of 4 months, starting on 1 August 2020 00:00, with the aim of producing a map of ASM for the *runoff* module.

A satellite-based estimation of the soil wetness, the Soil Water Index (SWI) proposed by Wagner et al. (1999), was used as initial condition on the warm-up module, as an independent source of information for the initial state of the warm-up period. The SWI, derived from the Surface Soil Moisture, is an exponential filter that, with a single parameter (here  $T = 20$ ), provides a trustworthy estimation of the relative soil moisture content in the root zone (Bouazziz et al., 2020; Brocca et al., 2011; Grillakis et al., 2016). These products are available since 2015 at the Land Copernicus Portal (<https://land.copernicus.eu/global/products/swi>) with 1 km<sup>2</sup> spatial resolution and daily temporal resolution (Bauer-Marschallinger et al., 2018). The SWI is provided as relative soil moisture content with respect to the wilting point (0%) and the field capacity (100%). Hence, it was used to compute the initial soil water content as:

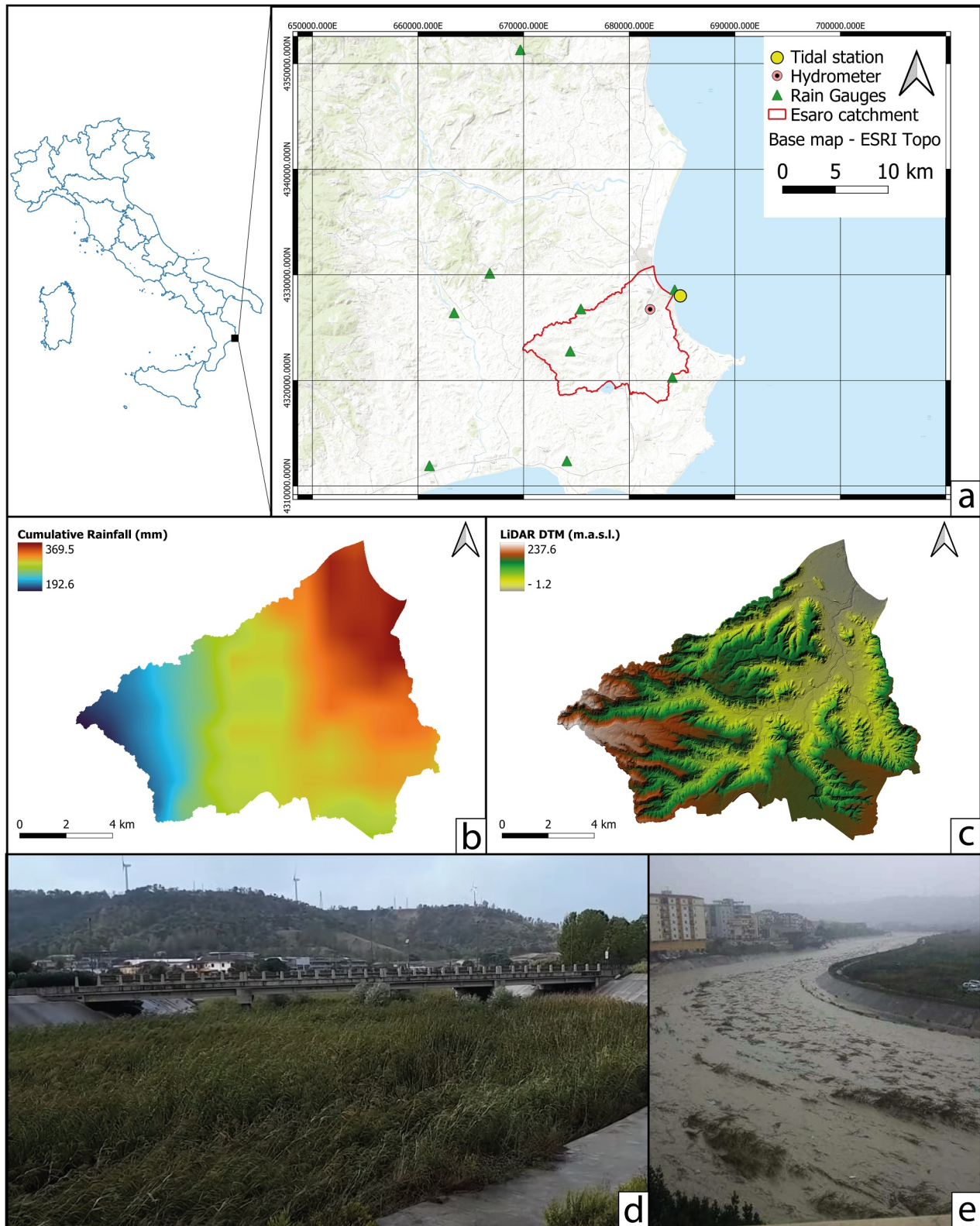


**Figure 3.** Study area: (a) Gauges locations; (b) Cumulated Rainfall derived from Rain Gauge-Radar merging (from 20 November 2020 00:00 to 24 November 2020 00:00); (c) Lidar-based digital elevation model; Esaro river vegetation state (d) 1 month before the flood event (e) during the flood event.

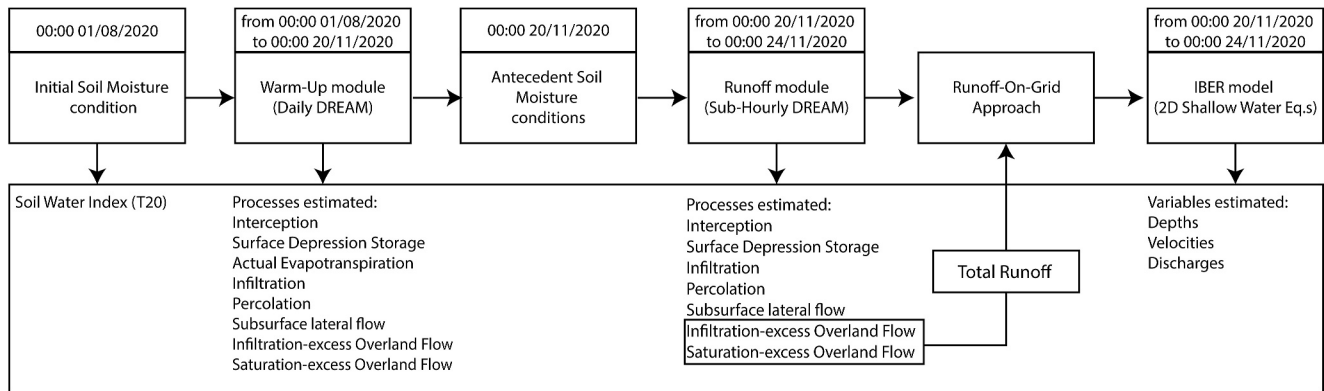


Figure 4. Workflow of the Runoff-On-Grid simulation.

$$S_{r,initial} = S_{wp} + SWI(S_c - S_{wp}) \quad (26)$$

The reference radar rainfall data used in this study were the Surface Rainfall Intensity (SRI) products obtained from the radar platform operated by the Italian National Department of Civil Protection platform (hereafter Radar-DPC) (Cimini et al., 2013), with 1 km<sup>2</sup> spatial resolution and 5 min' temporal resolution. The SRI data were aggregated to 24 hr and 15 min respectively for the warm-up module and for the *runoff* module. As already noted in the literature (Goudenhoofd & Delobbe, 2009; Jewell & Gaussiat, 2015; Nanding et al., 2015), this type of data is the most adequate to describe the spatiotemporal distribution of rainfall, but may not accurately capture the real values of rainfall. Given such a limitation, the radar products were adjusted with the nearest rain-gauge measurements (locations reported in Figure 3a) provided by CFM-ARPACAL. The in-situ observations were merged with the radar product (Figure 3b) using the Kriging with External Drift geostatistical interpolation, performed with the autoKrig function of the R automap package (Hiemstra et al., 2009). The potential evapotranspiration was computed following the Penman-Monteith equation, modified by the FAO procedure (Allen et al., 1998) that provides a simple means of studying the surface energy budget (Bonan, 2015). The site-specific solar radiation parametrization of the Ågnström–Prescott formula (Ågnström, 1924; Prescott, 1940) used in the FAO procedure was estimated following Guerrini et al. (1977) and Viglione et al. (2007). The schematic representation of the workflow used for the implementation of the Runoff-On-Grid methodology is shown in Figure 4.

For this application we exploited the finest high-resolution data freely accessible, as well as site-specific data provided upon request by the local authorities. Several data sources comprising the entire time span of the warm-up and runoff periods were implemented to describe the hydro-pedological characterization of the Esaro river basin. All the information relating to the products used in the present paper are reported in Table 1.

To lighten the computational cost without sacrificing an accurate spatial representation of the hydrological processes, the spatial discretization used in DREAM and Iber followed different criteria. A uniform 20 m grid discretization was used in the DREAM model, using twelve sub-catchments with an area ranging from 13.5 to 4.7 km<sup>2</sup> for the redistribution mechanisms already mentioned. The Iber model employed a non-uniform unstructured discretization with 1.23 million elements. The mesh size, as depicted in Figure 5a, was defined considering the expected volumes of total runoff to be routed. Indeed, the resolution progressively increases with respect to the hillslopes peripheral areas (20 m), giving priority to: areas with shallow rooting depths (15 m) since the soil bucket, in accordance with the DREAM model's design, quickly attains saturation; areas already mapped with different probabilities of flood hazard (10 m); and finally the finest mesh (from 2 to 5 m) in rivers and streams where potential overflowing and concatenated phenomena are expected. All building footprints were excluded from the numerical domain and were represented as holes in the computational mesh, following the building-hole approach (Cea, Garrido, & Puertas, 2010). A tidal downstream boundary condition was imposed along the whole seafront border, using the sea surface elevation registered at the Crotona Port station (location reported in Figure 3a), published by the Rete Mareografica Nazionale, an institution belonging to the Istituto Superiore per la Protezione e la Ricerca Ambientale (ISPRA).

**Table 1**  
*Data Sets and Products Used in the Study for the Construction of the Models Data Layers*

Variable	Data set	Resolution	Reference/source	License
Initial Soil Moisture condition (1 August 2020)	Soil Water Index ( $T = 20$ )	1 km, 1 day	<a href="https://land.copernicus.eu/global/products/swi">https://land.copernicus.eu/global/products/swi</a> ; Bauer-Marschallinger et al. (2018)	Open
Land Use	Corine Land Cover 2018	1:100,000	<a href="https://land.copernicus.eu/pan-european/corine-land-cover/clic2018">https://land.copernicus.eu/pan-european/corine-land-cover/clic2018</a>	Open
Leaf Area Index	MODIS—LAI MCD15A3H v061	0.5 km, 4 days	<a href="https://lpdaac.usgs.gov/products/mcd15a3hv061/">https://lpdaac.usgs.gov/products/mcd15a3hv061/</a> ; Myneni et al. (2021)	Open
Reference Soil depth	Soil rooting depth of Italy	1:250,000	<a href="https://zenodo.org/record/6926872">https://zenodo.org/record/6926872</a> ; Rivieccio et al. (2020)	Open
Topography	LIDAR-based Digital Terrain Model	1 m	<a href="mailto:datapst@mase.gov.it">datapst@mase.gov.it</a>	Upon request
Radar-Rainfall	Radar-DPC platform	1 km, 5 min	<a href="https://mappe.protezionecivile.gov.it/it/mappe-rischi/piattaforma-radar/">https://mappe.protezionecivile.gov.it/it/mappe-rischi/piattaforma-radar/</a>	Upon request
Rain-gauge Rainfall	CFM-ARPACAL	5 min	<a href="https://www.cfd.calabria.it/">https://www.cfd.calabria.it/</a>	Upon request
Temperature	Radar-DPC platform	1 km, 10 min	<a href="https://mappe.protezionecivile.gov.it/it/mappe-rischi/piattaforma-radar/">https://mappe.protezionecivile.gov.it/it/mappe-rischi/piattaforma-radar/</a>	Upon request
Wind Speed	ERA5—Land reanalysis	9 km, 1 day	<a href="https://cds.climate.copernicus.eu/cdsapp#/dataset/10.24381/cds.e2161bac?tab=overview">https://cds.climate.copernicus.eu/cdsapp#/dataset/10.24381/cds.e2161bac?tab=overview</a> ; Muñoz-Sabater et al. (2021)	Open
USDA Soil type, Percentage of sand, clay	LUCAS database	0.5 km	<a href="https://esdac.jrc.ec.europa.eu/content/lucas-2018-topsoil-data">https://esdac.jrc.ec.europa.eu/content/lucas-2018-topsoil-data</a> ; Ballabio et al. (2016)	Upon request
Organic matter	LUCAS database	0.5 km	<a href="https://esdac.jrc.ec.europa.eu/content/topsoil-soil-organic-carbon-lucas-eu25">https://esdac.jrc.ec.europa.eu/content/topsoil-soil-organic-carbon-lucas-eu25</a> ; de Brogniez et al. (2015)	Upon request
Building footprint	Carta Tecnica Regionale Calabria	1:5,000	<a href="http://geoportale.regione.calabria.it/">http://geoportale.regione.calabria.it/</a>	Upon request
Tidal level—Crotone Port	Rete Mareografica Nazionale—ISPRA	10 min	<a href="https://www.mareografico.it/">https://www.mareografico.it/</a>	Open
Water depths—Bridge San Francesco (Esaro River)	CFM-ARPACAL	1.5 min	<a href="https://www.cfd.calabria.it/">https://www.cfd.calabria.it/</a>	Upon request
Curve Number map	GCN250	250 m	<a href="https://doi.org/10.6084/m9.figshare.7756202.v1">https://doi.org/10.6084/m9.figshare.7756202.v1</a> ; Jaafar et al. (2019)	Open

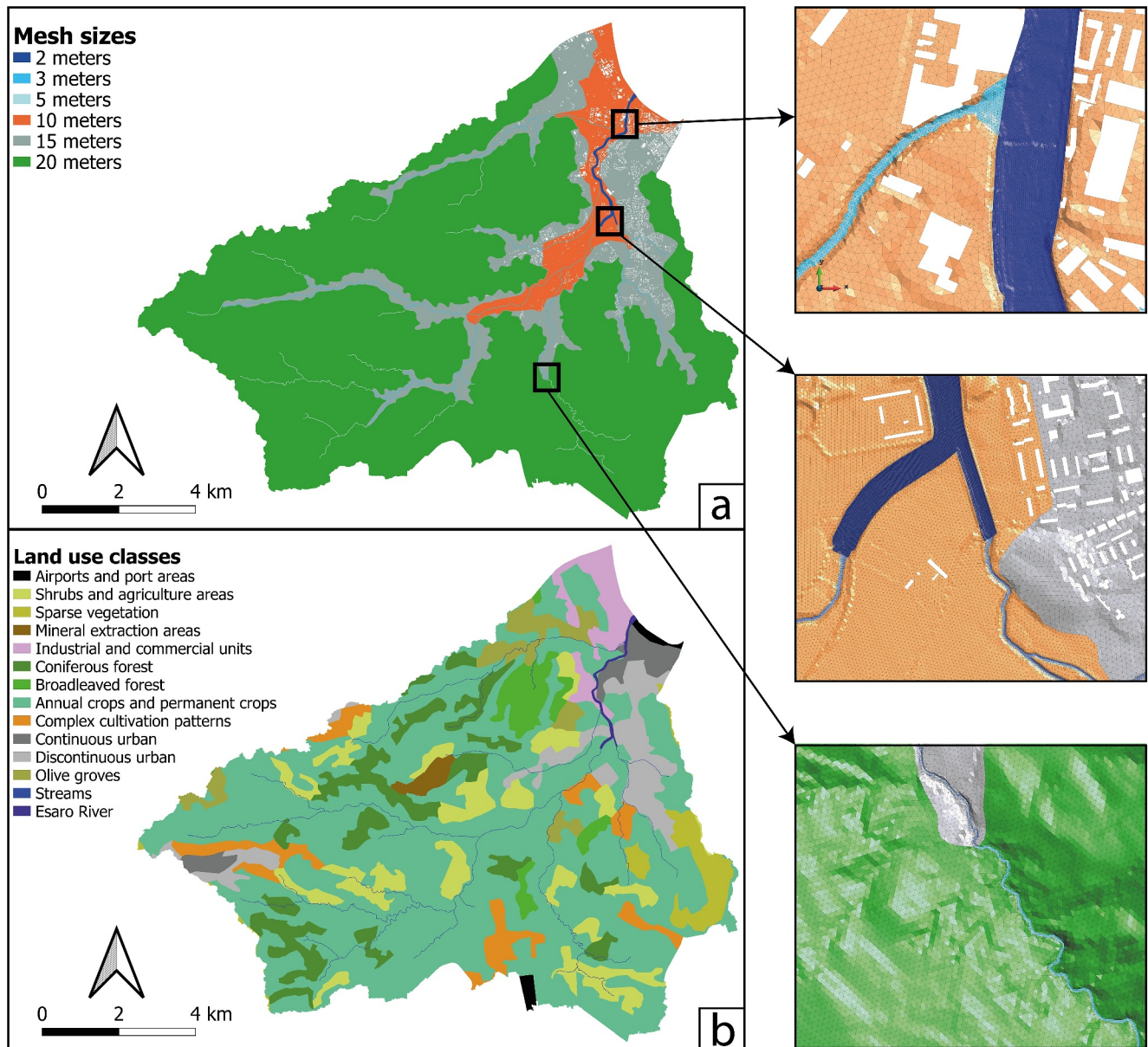


**Figure 5.** Details of the Iber model setup: (a) spatial discretization and mesh sizes, (b) land use classes. The insets offer an enlarged depiction of the mesh utilized in the Iber model.

### 3.2. Calibration Strategy of the Coupled DREAM-Iber Model

To minimize equifinality concerns only a limited number of all the available parameters in the coupled DREAM-Iber model was calibrated. It is important to underline that only the DREAM-related parameters ( $\alpha$ ; Equation 7 and  $c$ ; Equation 21) control the volume of total surface runoff. The Iber-related parameter ( $n$ ; Equations 24 and 25) controls the shape and the timing of the flow hydrographs and water depths, but not the volume of surface runoff.

The proposed modeling approach was tested against the water-levels registered at the Bridge San Francesco hydrometer, these provided by CFM-ARPACAL (location reported in Figure 3a). The available measurements spanned 2 days, 21 and 22 November 2020, during which three significant consecutive water level peaks were recorded on the first day, followed by lower peaks observed until the end of the second day. To address the potential inconsistencies between the LiDAR derived and the actual bathymetry of the Esaro river, the water

**Table 2**  
*Description of DREAM Parameters*

Parameter	Reference	Description	Spatially	Mean value or range
$S_r$	Rawls et al. (1982)	Fixed	Distributed	15 (%)
$S_{wp}$	Saxton and Rawls (2006)	Fixed	Distributed	44 (%)
$S_c$	Saxton and Rawls (2006)	Fixed	Distributed	76 (%)
$K_s$	Saxton and Rawls (2006)	Fixed	Distributed	6.7 (mm/hr)
$a$	Dickinson (1984)	Fixed	Lumped	0.2 (–)
$\mu$	Larcher (1975)	Fixed	Distributed	0.35–0.66 (–)
$W_{dep\_max}$	Liu and De Smedt (2004)	Fixed	Distributed	0.97 (mm)
$C_p$	Liu and De Smedt (2004)	Fixed	Distributed	0.63 (–)
$\alpha$	Liu and De Smedt (2004)	Calibration	Lumped	0–3 (–)
$c$	Manfreda et al. (2005)	Calibration	Lumped	0–1 ( $T^{-1}$ )
$m$	Rawls and Brakensiek (1985)	Fixed	Distributed	0.35 (–)

levels were converted into Water Surface Elevation (WSE) using on-site information related to the hydrometer's zero elevation during this flood event provided by CFM-ARPACAL. The evaluation of the performance metrics conducted on the WSE time series bypasses the determination of flow rating curves, which are considered a prerequisite for traditional rainfall-runoff models.

All the fixed and variable hydrological parameters of the catchment are reported in Table 2, while the roughness coefficients were assigned by taking into account the physical conditions of the several land use classes present in the catchment (Figure 5b), along ranges of values proposed in Arcement and Schneider (1989), Barnes (1967), Brunner (2016), Chow (1959), and Engman (1986). Following a series of preliminary tests, it was found that the water depth at the gauge station was not sensitive to all the roughness coefficients and thus, only the local coefficient associated to the Esaro River and the coefficients of land use classes covering a substantial portion of the catchment were subject to calibration (Table 3). The range adopted for the Esaro river was defined considering the strong obstruction of the dense reeds (Figure 3d) which also had a relevant impact during the event (Figure 3e). Thus, for the specific hindcast we chose a range of variation of the Manning roughness coefficient from 0.1 to  $0.2 \text{ m}^{-1/3} \text{ s}$  corresponding to “extreme amount of vegetation” in Arcement and Schneider (1989).

**Table 3**  
*Calibrated Manning Coefficients*

Land use classes	$n$ Range of variation ( $\text{m}^{-1/3} \text{ s}$ )	$n$ ( $\text{m}^{-1/3} \text{ s}$ )
Airports and port areas	Not calibrated	0.054
Shrub and agriculture areas	0.0350–0.070	0.035
Sparse vegetation	0.0350–0.070	0.050
Mineral extraction areas	Not calibrated	0.140
Industrial or commercial units	Not calibrated	0.150
Coniferous forest	Not calibrated	0.110
Broadleaved forest	Not calibrated	0.100
Annual crops and permanent crops	0.030–0.050	0.035
Esaro River	0.100–0.200	0.100
Streams	Not calibrated	0.033
Olive groves	Not calibrated	0.080
Complex cultivation	0.030–0.050	0.040
Continuous urban	Not calibrated	0.100
Discontinuous urban	Not calibrated	0.060

The calibration was achieved progressively by selecting the set of parameters that maximize the KGE coefficient (Gupta et al., 2009), exploiting an iterative approach that prioritized first the two lumped hydrological parameters and then the distributed Manning coefficient. In scenarios where extensive data sets are available, this type of simulator favors the actuation of multiple sources of validation, such as operational testing with space-time hydrological measurements (Dal Molin et al., 2020; Fenicia et al., 2022), but emerging satellite techniques can also be used as a reference of flood extent for the validation of hydrodynamic outcomes (Albertini et al., 2022; Cea et al., 2024; Di Baldassarre et al., 2009; Masafu & Williams, 2024; Schumann & Moller, 2015).

## 4. Results and Discussion

Generally speaking, calibrating hydrological models for high and low peaks simultaneously to adequately represent all phases with the same parameter set is a challenging task, since several surface and soil processes can be involved (Madsen, 2000; Pfannerstill et al., 2014). This event was used to test the structure of the model, also by comparison to other modeling hypothesis, and their parameterization. The best numerical-experimental agreement of the DREAM-Iber model attains an efficiency of 0.96 (Figure 8a). This performance is obtained by attenuating the infiltration excess parameter ( $\alpha = 1.35$ ), maximizing the coefficient that regulates the saturation excess exfiltration ( $c = 1$ ), and calibrating the Manning coefficients, as reported in Table 3.

The physical interpretation of the Manning coefficient helped to select exclusively those parameters with a reasonable range of variation, bypassing equifinality problems that in distributed complex hydrological-hydrodynamic models are endemic and thus always expected (Herrera et al., 2022; Kirchner, 2006). All the simulations conducted in this hindcasting were significant quickened exploiting the GPU parallelized Iber+ on the resources of the ReCas HPC Cluster. As a result, the computational efficiency of the system enables us to simulate nearly 4 days of real-time in just 1 hr and 10 min (4,241 s), more than 80 times faster than real time.

The results of the different stages of the Runoff-On-Grid application conducted with the DREAM model, even compared with other model structures, are described in Sections 4.1, 4.2 and 4.3. A qualitative validation of the flood extent simulated by the DREAM model is shown in Section 4.4. Finally, a comparison with the FHA exploiting the Soil Conservation Service Curve Number (CN) method is presented in Section 4.5.

### 4.1. Warm-Up Module Results

The catchment-averaged relative soil moisture condition on 1 August 2020 00:00, as derived from the SWI, was 52.4%, which is near the wilting point ( $S_{wp}$ ), thus indicating a low water content, particularly for vegetation water uptake. Thus, the water-budget for the entire warm-up period was strongly controlled by the actual evapotranspiration from the soil ( $ET_{soil}$ ), which turned out to be much lower than the potential evapotranspiration (EP) (Figure 6a). The values of infiltration-excess OF, saturation-excess OF, and percolation were almost null in the warm-up period, since the two threshold mechanisms (related to the hydraulic conductivity (Equation 7) and to the soil moisture content at field capacity (Equations 20 and 21)), were mostly not exceeded during the entire period throughout the basin. The propaedeutic reconstruction of the ASM conditions on 20 November 2020 00:00 resulted in a slightly higher wetness state still between the wilting point and the field capacity (59.8%). Other warm up periods (shorter than 4 months) were also tested a posteriori, starting from different SWI images closer to the flood event. It was found that the ASM obtained at the end of the warm-up period was not completely independent from the warm-up initial conditions, nevertheless the performances of the hydrologic-hydrodynamic model were always acceptable.

### 4.2. Runoff Module Results

The relatively low ASM on 20 November 2020 00:00 attenuated the meteorological event's impact, leading to a significant lamination effect during the first stages of the storm (Figure 6b) in which the only source of surface runoff was the infiltration-excess OF. Subsequently, soil water was released as saturation-excess OF only during the rainfall peaks of 21 November 2020 (i.e., ~10 hr after the start of the rainfall), after the field capacity was exceeded. For the latter days of the simulation the most consistent source of runoff from the saturation excess OF, since the topsoil saturated conductivity threshold was mostly not exceeded while subsurface processes were still activated. Although the catchment-averaged rates of saturation-excess runoff are one order of magnitude lower than those of infiltration-excess, it is important to note that the redistribution equation (Equation 20) favors the exfiltration in those cells with a high TWI. Indeed, only locations near the stream network contribute to this

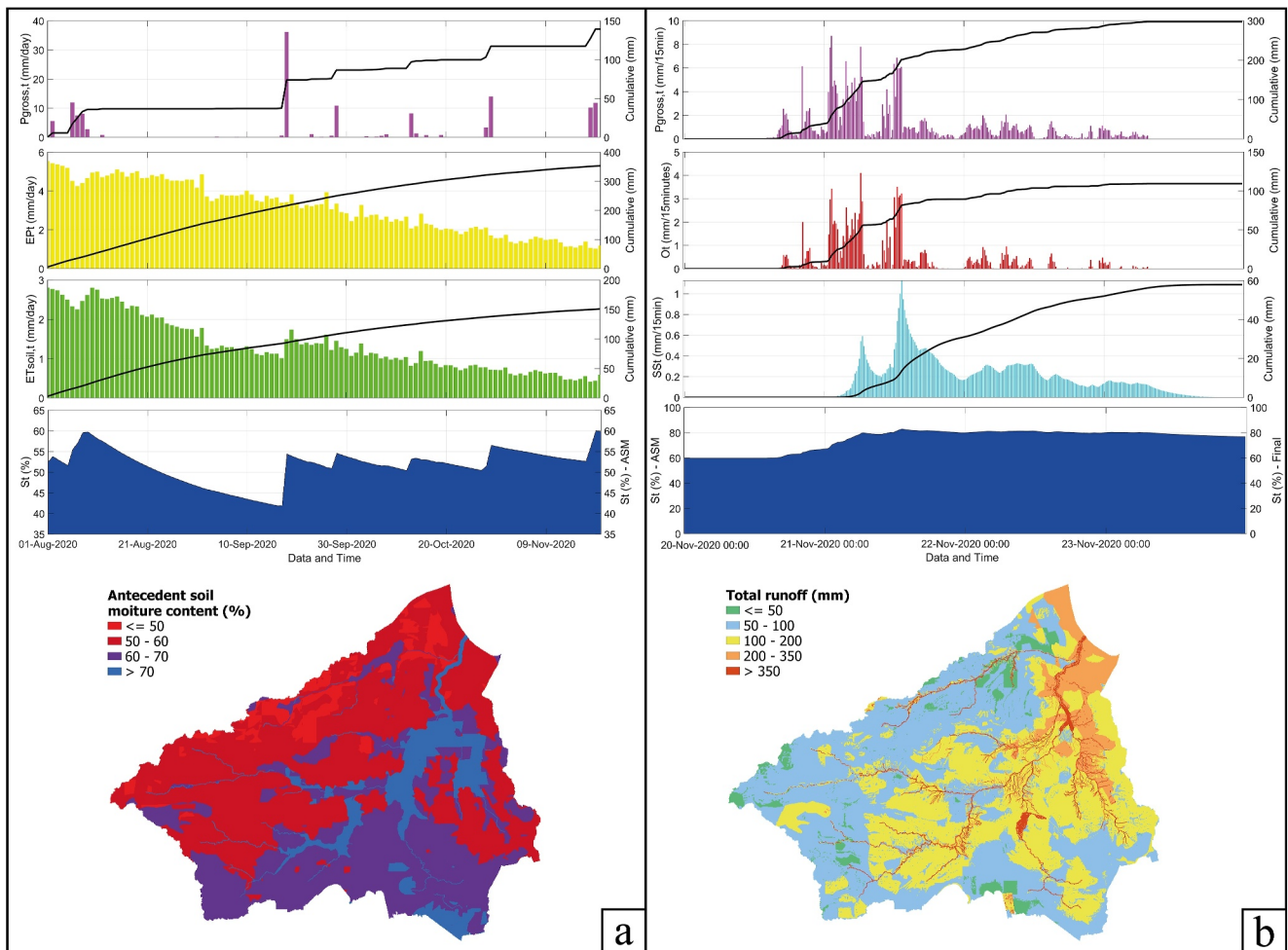


**Figure 6.** DREAM model results (a) warm-up module (b) *runoff* module. All the variables reported in the figure follow the same nomenclature reported in the equations of Section 2.

process, while a large portion of the catchment does not directly produce any saturation-excess OF. This results in concentrated volumes of exfiltration markedly higher than those produced by the infiltration-excess mechanism that represent relevant and non-negligible volumes to be routed with the hydrodynamic model. The cumulated total runoff depths consistently exceed the local gross precipitation within the same time step, and exfiltration from the soil is also observed in the absence of rainfall. These observations provide valuable insights into soil water dynamics during and after storm events that cannot be observed when relying on the event-based empirical loss methods used in FHA.

To assess the necessity to consider the multiple runoff sources simulated by the *runoff* module, we tested separately the performance of the DREAM model either considering only Hortonian OF or Dunnian OF. The Hortonian OF was obtained by assuming a null redistribution coefficient without altering the other parameters. The Dunnian OF output was produced by activating runoff production only when soil-bucket capacity was exceeded that is, in the form of saturation-excess OF. Both these two alternative DREAM structures, coupled with the Iber model, are referred to the Hortonian and Dunnian models in the subsequent section.

### 4.3. Hydrological-Hydrodynamic Results

The steep topographic gradients, together with both the presence of impervious surfaces and the poor management of the open channel, produced a rapid response in the catchment, triggering river overflowing at multiple locations in the city of Crotona. As depicted in Figure 7a, the DREAM-Iber model results show a remarkable



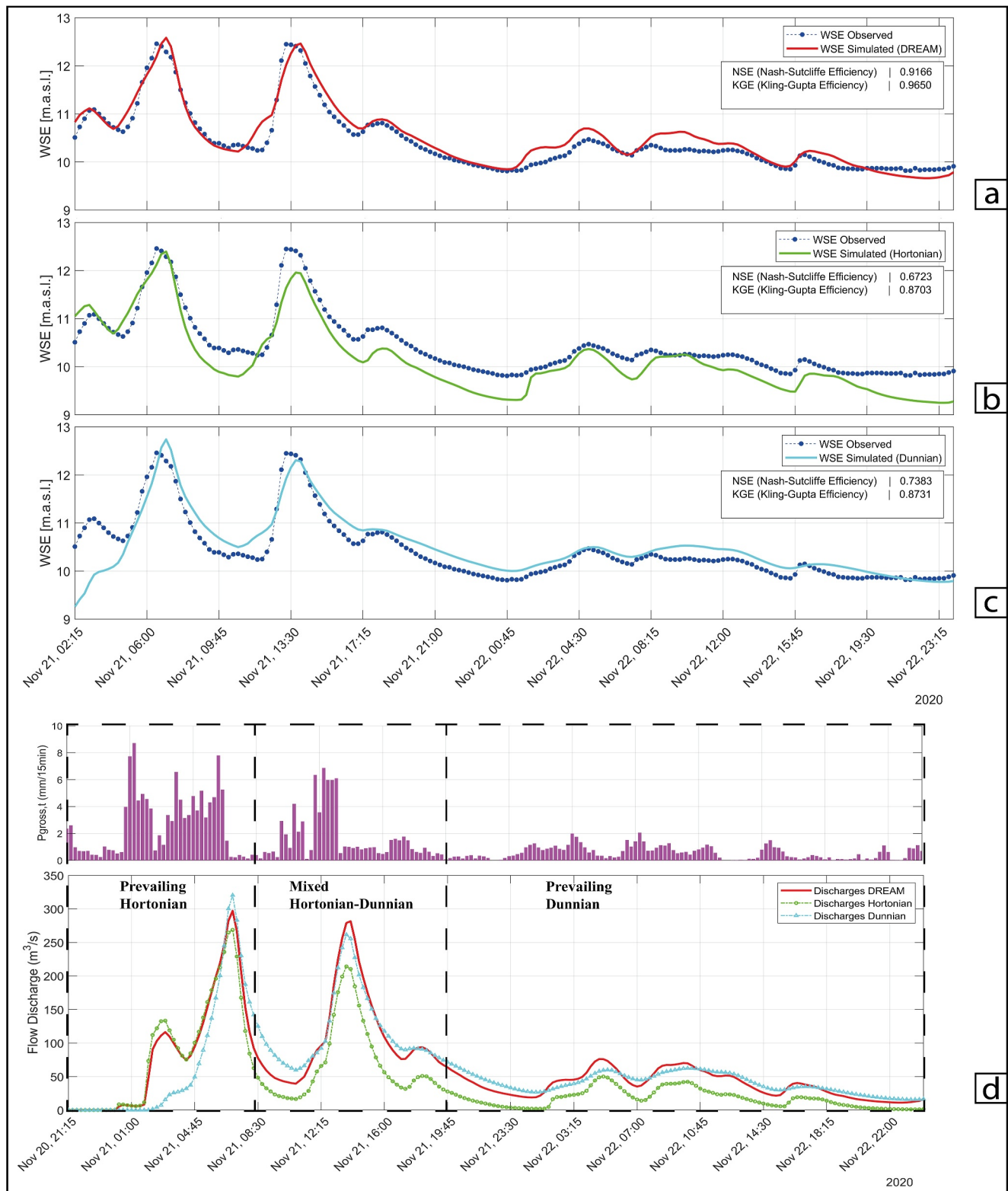


**Figure 7.** Iber model results referred to the Runoff-On-Grid application: (a) DREAM model performance, (b) Hortonian model performance, (c) Dunnian model performance, (d) Flow discharges simulated and dominant mechanisms of runoff for the different stages of the simulation.

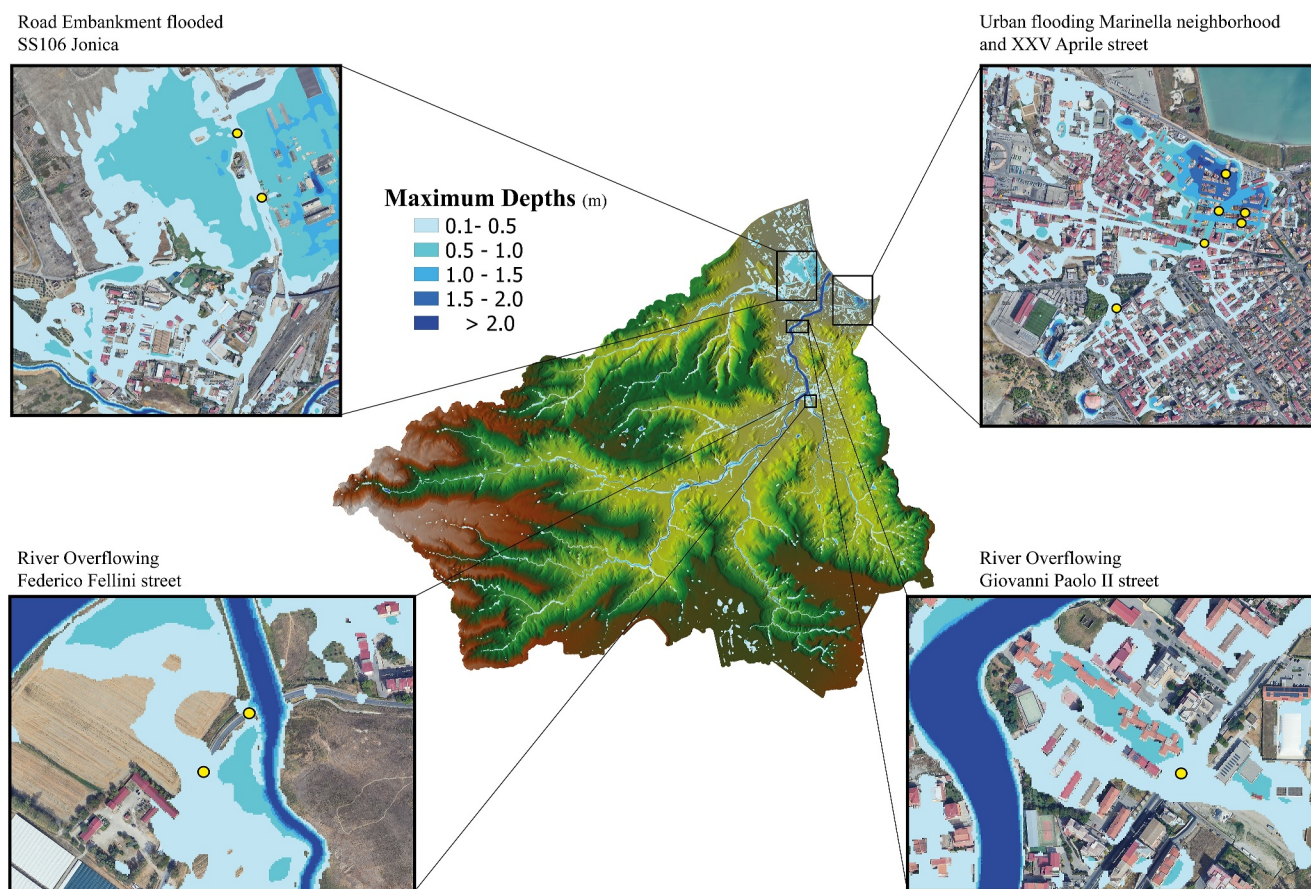


**Figure 8.** Flood Extent (maximum envelope of the depths from 20 November 2020 00:00 to 22 November 2020 00:00); the yellow dots represent the exact location in which different types of flooding were documented through the CNR-report or by means of specific photos taken on 21 November 2020.

graphical agreement and performance metrics with respect to the observed WSE, reaching a KGE of 0.96 and a Nash-Sutcliffe efficiency of 0.91.

Therefore, we tested the alternative DREAM structures by routing the single-type OF in Iber. The Hortonian model (Figure 7b) closely mirrors the complete *runoff* module, albeit with a slightly higher initial low peak, until the decay stage of the second peak producing a generalized underestimation of water stages for the rest of the event. Conversely, the Dunnian model hydrograph (Figure 7c) entirely loses the first (low) peak and slightly overestimates and delays the second peak, indicating structural deficiencies in describing the early stages of the flood event. It is worth noting that the initial low peak corresponds to the highest rainfall intensity, whereas the subsequent high peaks are triggered by lower rainfall intensities.

In practice, none of the specific OFs is able to reproduce the entire event as satisfactory as the complete *runoff* module.

Nevertheless, these results show that the Hortonian OF can capture the immediate response of the basin, responsible of the first two peaks, but loses the hydrological response in following ones, including the third high peak. Conversely the Dunnian OF is essential to obtain good model performances for most of the simulated event from the recession limb of the second peak to the end. Indeed, for the Dunnian model the volume underestimation attains 3%, while the Hortonian model produces a 44% underestimation (Table 4).

Overall, the first two peaks were dominated by Hortonian mechanisms, while lower peaks on the 22 November 2020 were mainly Dunnian-driven. Both single-type of OF models, separately, underestimate the third high peak, underscoring the necessity of both processes modeled in the complete DREAM. This assessment is visually depicted in Figure 7d, delineating three macro-periods with associated prevailing runoff mechanisms.

**Table 4**  
*Metrics Performance, Peaks Discharges and Volumes of the Different Model Output*

Model	KGE	NSE	Second peak discharge (m <sup>3</sup> /s)	Third peak discharge (m <sup>3</sup> /s)	Cumulative volumes (DREAM as benchmark) (%)
DREAM	0.965	0.916	297	281	–
Hortonian model	0.870	0.672	268 (–10%)	214 (–24%)	–44
Dunnian model	0.873	0.738	320 (+7%)	261 (–12%)	–3
CN-std	0.712	0.564	416 (+40%)	351 (+25%)	+29
CN-cal	0.894	0.825	328 (+10%)	292 (+4%)	+4

#### 4.4. Qualitative Validation

The flood extent predicted with the DREAM-Iber model (Figure 8) shows multiple overflowing spots along the Esaro river. A significant part of the inundation is generated by local accumulation of the total runoff in urban areas, which should formally be classified as a source of pluvial hazard. A comprehensive numerical assessment in terms of performance metrics of the hydrodynamic results was not possible due to the lack of complete and detailed validation data. Still, a qualitative validation was carried out by exploiting non-conventional data such as photographs and news reports, as advocated by Macchione et al. (2019). Considering that the Runoff-On-Grid approach allows for the identification of all the flood prone areas along the whole computational domain, any kind of spatiotemporal information acquired during the flood is a potential data source for model validation.

The two sources of information used for the validation in this study were the post-event report by CNR-Irpi (which collects information from several sources of local, regional and national reports and media outlets) and a collection of helicopter and amateur photographs taken on 21 November 2020. It should be noted that precise temporal information pertaining to the photographs was unavailable. Thus, the comparison was undertaken using the maximum flood extent predicted till the end of 21 November 2020. For the visualization of the flood extent, all the regions in the numerical results with a water depth lower than 10 cm were filtered. All the information certified by CNR-Irpi, concerning the flooded areas observed in different parts of the catchment and represented as yellow markers in the insets of Figure 8, were successfully replicated by the model. This information pertains to two instances of the overflowing of the Esaro river, the inundation of the road embankment and the substantial accumulation of water within the city center of Crotona.

Also, four reference photographs were graphically compared to a three-dimensional virtual reality representation of the simulated water level using Google Earth Pro (Figure 9). Some possible explanations of the discrepancies observed (over/under-estimation) can be related to the reference numerical map, the “unreal” filtering technique on



**Figure 9.** 3-D graphical comparison between real flooding photographs and simulated flood extent (maximum envelope of the depths from 20 November 2020 00:00 to 22 November 2020 00:00).

the depths, and the inexact local rainfall-runoff transformations. However, all the information gathered appeared to be in line with the numerical results, although it is difficult to give precise and reliable performance measures.

#### 4.5. Comparison With the Soil Conservation Service Curve Number Method

To test the advancements of the hydrological-hydrodynamic approach presented here, we conducted a comparison with other commonly used FHA approaches. In particular, we applied the widely accepted Soil Conservation Service—Curve Number (SCS-CN) method for net rainfall evaluation, which was used in other event-based hydrological simulations of floods within the Iber software (Cea et al., 2022, 2024).

The conceptual formulation of the SCS-CN has not been reported here for the sake of conciseness, the reader can refer to USDA NRCS (2004). For the present application, the reference CN maps used to estimate the potential infiltration are the global GCN250 (Jaafar et al., 2019) which are based on the original CN tables (USDA NRCS, 2004).

The SCS-CN methodology was applied considering the 5 days antecedent rainfall depth (i.e., ~22 mm), resulting in a medium Antecedent Runoff Condition (ARCI) for the dormant season (Silveira et al., 2000), with a catchment-averaged CN of 77.

The SCS-CN method under standard conditions (CNstd model) showed a significant overestimation across all target measurements (Figure 10a). In particular, the overestimation compared to the DREAM model reaches 40% and 25%, respectively, for the second and third peak discharges, and 29% in terms of cumulative volumes crossing the gauge location (Table 4 and Figure 10d). This is not surprising considering that they were obtained using the tabulated NRCS CN values, which are rarely applicable a priori (Assaye et al., 2021; Tedela et al., 2012; Walega et al., 2020).

Therefore, we performed a calibration (hereafter CNcal model) maximizing the KGE, varying both the CN values (here with a multiplier  $\varepsilon$ ) and the initial abstraction ratio ( $0.0 \leq \lambda \leq 0.3$ ). The best fit reaches a KGE of 0.89 employing a  $\lambda$  of 0.0 and a  $\varepsilon$  of 0.75 (Figure 10b).

The null value of  $\lambda$  obtained after calibration physically represents zero initial losses due to interception and surface storage, which is evidently unrealistic. The spatial average of the calibrated CN (i.e., 57.7) turns out to be lower than the one corresponding to the ARCI (i.e., 59). The latter is conventionally assumed to be equal to a soil state coincident to the wilting point (Hawkins et al., 2008) which is considered the lowest technical ARC value. Such result is also quite far from the ARCI condition, dependent on the precipitation observed in the 5 days before the flood event, whose relatively simple evaluation makes the SCS-CN procedure widespread for engineering purposes. Moreover, the ARC condition associated to the CNcal model is not consistent with the ASM estimated with the warm-up model supported by satellite SWI observations.

Notwithstanding the good KGE value reached after model calibration, the rising limb of the first (low) peak is underestimated while the second peak of the event is still quite overestimated. With reference to the multiple peaks of the 22 November 2020, the CNcal model shows irregular and overestimating low peaks when compared to the smoother observed ones. These findings may suggest a deficit in the model structure (Pfannerstill et al., 2014), since also after the calibration these patterns remained fairly unchanged.

Low peaks are generally heavily controlled by soil processes that are not explicitly assessed into the SCS-CN formulation, which was not conceived to consider the evolution of the hydrological state of the catchment. Although the global performance of the CNcal results are in a satisfying range, these metrics are dominated by high flows, which masks the poor performance during low flow periods (Krause et al., 2005; Zhang et al., 2011). Focusing on the KGE performances in a limited time span the CNcal model shows deteriorated performance of 0.13 (Figure 10c), while the DREAM model reaches 0.62. This reveals, particularly for the SCS-CN formulation an attitude to reproduce accurately only the high-flow stages of the simulation. At this point, it is worth to mention that the original SCS-CN procedure was developed as a spatially lumped model, to convert part of the daily rainfall depth in direct runoff depth or net rainfall (Mockus, 1964; Ponce & Hawkins, 1996). Indeed, simulating rainfall-runoff transformation in a fully distributed manner with sub-hourly time integration through a 2D-SWE model extends beyond the original applicability of the SCS-CN method.

Overall, this comparison serves to highlight some of the breakthroughs that can be achieved in catchment-scale modeling using the Runoff-on-Grid approach when compared to the classic Rain-on-Grid method.

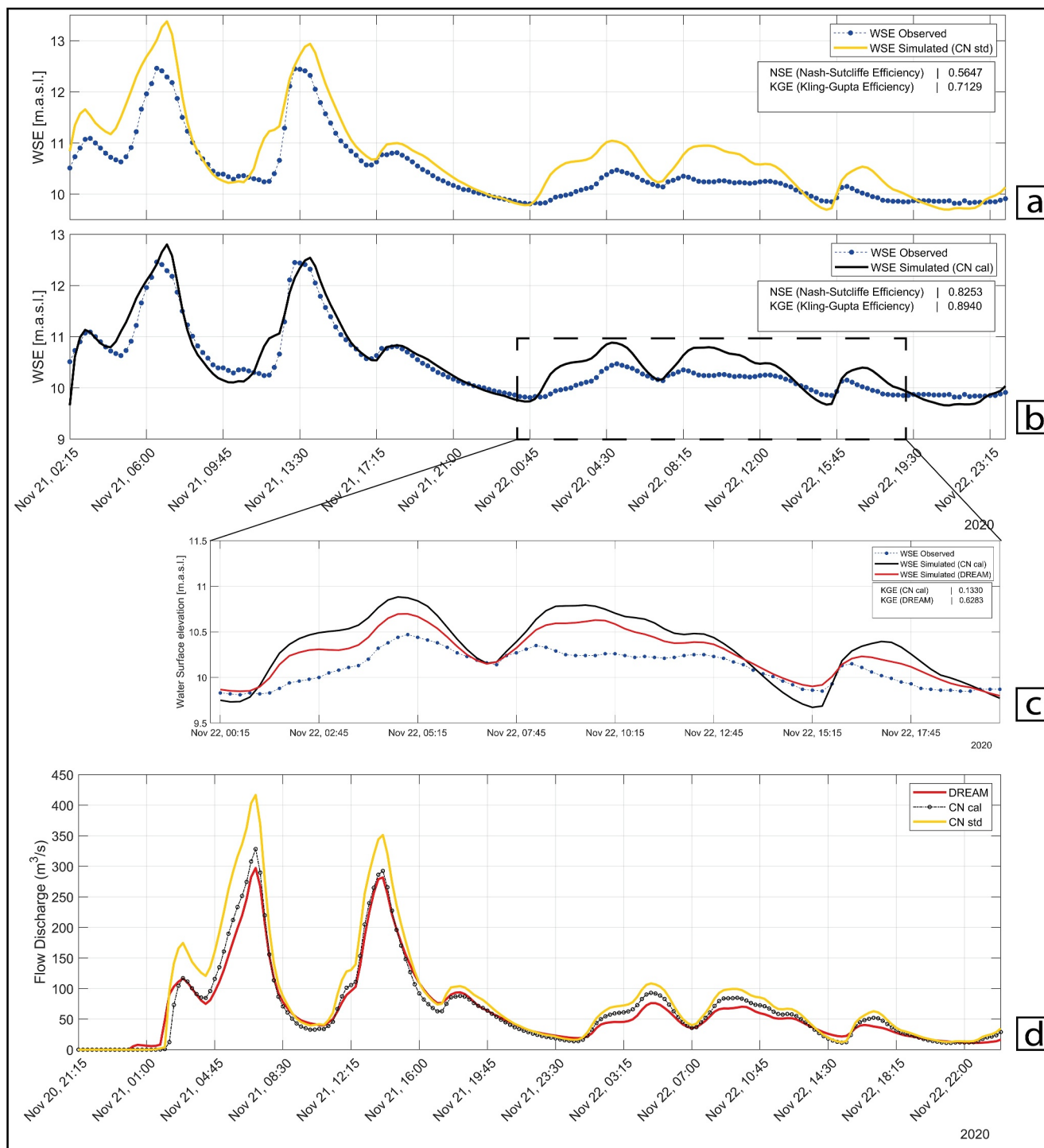


**Figure 10.** Iber model results referred to the Soil Conservation Service—Curve Number application: (a) CNstd model performance, (b) CNcal model performance, (c) low peaks performance of DREAM and CNcal models, (d) Flow discharges of the CNcal, CNstd and DREAM models.

## 5. Conclusions

We introduced a new way to extend hydrodynamic models based on the 2D shallow water equations to physically-based hydrological modeling, exploiting a methodology called Runoff-on-Grid. This new approach combines a topsoil hydro-pedological characterization of the catchment with fully-dynamic wave equations, embedding subsurface processes and soil physics into the coupled hydrological-hydrodynamic modeling.

Avoiding some limitations of the traditional loss approaches used in FHA, the Runoff-On-Grid method opens up new insights relating to the exploitation of 2D depth-averaged shallow water equation models for testing runoff generation sources. The results obtained on a single hindcasting event are very encouraging, although they need to be further examined and assessed in subsequent studies.

The two numerical models involved in this study (Iber and DREAM) benefit from the coupling. Nonetheless, the Runoff-On-Grid approach is not aligned exclusively with these two models.

The results presented here demonstrate that well-established initial and boundary conditions, generated with enabling technologies and unconventional data sources, support the description of flood-induced processes, thus enhancing the reconstruction of extreme events.

By comparing different hydrological model structures, we assessed the dominant runoff sources on the different stages of the flood, while we identified some limitations of the SCS-CN method when employed with the FHA. Furthermore, it emerges that for a relatively small increase or decrease in reference performance metrics profound structural difference of hydrological models can be hidden.

The procedures adopted in this paper for calibration and validation of the DREAM-Iber model do not allow to consider the model structure and parameterization of general applicability. While results are consistent with available observations, a complete model validation and assessment should involve its application to more events. Nonetheless, being the model parameterization strongly based on physical features of the basin, it is suitable for a continuous model assessment based on monitoring of the Esaro river conditions. This provides the structure of the DREAM-Iber model to be potentially representative of future scenarios and suitable for different applications from nowcasting to climate change impact studies.

The efficiency of the HPC framework used in this study also shows the effectiveness of using the proposed approach for multi-objective nowcasting. Indeed, contrary to the uncoupled models, the system could provide flood forecast based on advanced hydrodynamics and a simultaneous root-zone hydrological budget. Therefore, the diverse capabilities unveiled through this methodology, contribute to an exciting effort in constructing unified frameworks for managing natural hazards, claimed as Digital Twins. If the objective is to improve flood hazard forecasting based on “scientific” assessment of the models (Biondi et al., 2012; Kirchner, 2006), a more conscious assessment of the inducing processes of the natural disaster is needed. In this context, the Runoff-On-Grid approach claims to be a potential breakthrough, in that it provides a simple way to integrate and test process-based hydrological knowledge into numerical hydrodynamic simulators. Thus, we envisage new perspectives on catchment scale modeling, in step with technological and computational innovations, for supporting climate change adaptation and advanced flood hazard prediction as subject of future research.

## Data Availability Statement

All the data used in the study are mentioned, described, and referenced in the manuscript (Table 1). The numerical simulations were done with the software Iber v3.2.2, which can be downloaded for free of charge from [www.iberaula.com](http://www.iberaula.com). The DREAM code (MATLAB script) exploited in this study is available upon request to the corresponding author.

## References

- Ångström, A. (1924). Solar and terrestrial radiation. *Monthly Weather Review*, 52(8), 397. [https://doi.org/10.1175/1520-0493\(1924\)52<397:satr>2.0.co;2](https://doi.org/10.1175/1520-0493(1924)52<397:satr>2.0.co;2)
- Albertini, C., Gioia, A., Iacobellis, V., & Manfreda, S. (2022). Detection of surface water and floods with multispectral satellites. *Remote Sensing*, 14(23), 6005. <https://doi.org/10.3390/rs14236005>
- Allen, R. G., Pereira, L. S., Raes, D., & Smith, M. (1998). FAO Irrigation and drainage paper No. 56. *Food and Agriculture Organization of the United Nations*, 56(97), e156.

### Acknowledgments

The manuscript contains part of the results of the Ph.D. research of P. Perrini, whose fellowship (CUP H99J21010150001 n° DOT20THYKL-4) is funded by PON project: “Programma Operativo Nazionale Ricerca e Innovazione 2014–2020, risorse FSE REACT-EU,—Azione IV.4—Dottorati di ricerca su tematiche dell’innovazione.” The study was supported by the financial resources of “National Center for HPC, Big Data and Quantum Computing Area tematica: Simulazioni, calcolo e analisi dei dati ad alte prestazioni PNRR MUR—M4C2—I 1.4” and the “RETURN Extended Partnership funded from the European Union Next-Generation EU (National Recovery and Resilience Plan—Mission 4, Component 2, Investment 1.3—D.D. 1243 2/8/2022, PE0000005).” This research was developed as side and preliminary investigations in carrying out the activities of the Flood Risk Management Plan in the fulfillment of the Operational Agreement between the Autorità di Bacino Distrettuale dell’Appennino Meridionale (ABDAM) and the Consorzio Interuniversitario per l’Idrologia (CINID). Hence, we thank Dr. Vera Corbelli for having inspired and encouraged the development of this work, Eng. Rocco Bonelli, Eng. Luciana Giuzio (ABDAM), and Professors Leonardo Cascini and Francesco Macchione for all fruitful discussions and suggestions. Finally, the authors are grateful to: Mermec Engineering s.r.l. (Noci (BA) Italy) for providing topographic data, CFM-ARPACAL for providing site-specific information useful for the present analysis, Maddalena Perrini for the original draft of Figure 1.

- Antonacci, M., Bellotti, R., Cafagna, F., de Palma, M., Diacono, D., Donvito, G., et al. (2017). The ReCaS project: The Bari infrastructure. In *High performance scientific computing using distributed infrastructures: Results and scientific applications derived from the Italian PON ReCaS Project* (pp. 17–33). World Scientific.
- Arcement, G. J., & Schneider, V. R. (1989). Guide for selecting Manning's roughness coefficients for natural channels and flood plains.
- Assaye, H., Nyssen, J., Poesen, J., Lemma, H., Meshesha, D. T., Wassie, A., et al. (2021). Curve number calibration for measuring impacts of land management in sub-humid Ethiopia. *Journal of Hydrology: Regional Studies*, 35, 100819. <https://doi.org/10.1016/j.ejrh.2021.100819>
- Ballabio, C., Panagos, P., & Monatanarella, L. (2016). Mapping topsoil physical properties at European scale using the LUCAS database. *Geoderma*, 261, 110–123. <https://doi.org/10.1016/j.geoderma.2015.07.006>
- Barbero, G., Costabile, P., Costanzo, C., Ferraro, D., & Petaccia, G. (2022). 2D hydrodynamic approach supporting evaluations of hydrological response in small watersheds: Implications for lag time estimation. *Journal of Hydrology*, 610(November 2021), 127870. <https://doi.org/10.1016/j.jhydrol.2022.127870>
- Barnes, H. H. (1967). *Roughness characteristics of natural channels*. (Issue 1849). US Government Printing Office.
- Bates, P. D., Quinn, N., Sampson, C., Smith, A., Wing, O., Sosa, J., et al. (2021). Combined modeling of US fluvial, pluvial, and coastal flood hazard under current and future climates. *Water Resources Research*, 57(2), e2020WR028673. <https://doi.org/10.1029/2020wr028673>
- Bauer-Marschallinger, B., Paulik, C., Hochstöger, S., Mistelbauer, T., Modanesi, S., Ciabatta, L., et al. (2018). Soil moisture from fusion of scatterometer and SAR: Closing the scale gap with temporal filtering. *Remote Sensing*, 10(7), 1030. <https://doi.org/10.3390/rs10071030>
- Betson, R. P. (1964). What is watershed runoff? *Journal of Geophysical Research*, 69(8), 1541–1552. <https://doi.org/10.1029/jz069i008p01541>
- Beven, K. (2007). Towards integrated environmental models of everywhere: Uncertainty, data and modelling as a learning process. *Hydrology and Earth System Sciences*, 11(1), 460–467. <https://doi.org/10.5194/hess-11-460-2007>
- Beven, K., & Germann, P. (2013). Macropores and water flow in soils revisited. *Water Resources Research*, 49(6), 3071–3092. <https://doi.org/10.1002/wrcr.20156>
- Beven, K. J. (2011). *Rainfall-runoff modelling: The primer*. John Wiley & Sons.
- Beven, K. J., & Alcock, R. E. (2012). Modelling everything everywhere: A new approach to decision-making for water management under uncertainty. *Freshwater Biology*, 57(SUPPL. 1), 124–132. <https://doi.org/10.1111/j.1365-2427.2011.02592.x>
- Beven, K. J., & Chappell, N. A. (2021). Perceptual perplexity and parameter parsimony. *Wiley Interdisciplinary Reviews: Water*, 8(4), e1530. <https://doi.org/10.1002/wat2.1530>
- Biondi, D., Freni, G., Iacobellis, V., Mascaro, G., & Montanari, A. (2012). Validation of hydrological models: Conceptual basis, methodological approaches and a proposal for a code of practice. *Physics and Chemistry of the Earth*, 42–44, 70–76. <https://doi.org/10.1016/j.pce.2011.07.037>
- Bladé, E., Cea, L., Corestein, G., Escolano, E., Puertas, J., Vázquez-Cendón, E., et al. (2014). Iber: Herramienta de simulación numérica del flujo en ríos. *Revista Internacional de Métodos Numéricos Para Cálculo y Diseño En Ingeniería*, 30(1), 1–10. <https://doi.org/10.1016/j.rimni.2012.07.004>
- Blair, G. S., Beven, K., Lamb, R., Bassett, R., Cauwenberghs, K., Hankin, B., et al. (2019). Models of everywhere revisited: A technological perspective. *Environmental Modelling & Software*, 122(September), 104521. <https://doi.org/10.1016/j.envsoft.2019.104521>
- Blöschl, G. (2022). Flood generation: Process patterns from the raindrop to the ocean. *Hydrology and Earth System Sciences*, 26(9), 2469–2480. <https://doi.org/10.5194/hess-26-2469-2022>
- Blöschl, G., Bierkens, M. F. P., Chambel, A., Cudennek, C., Destouni, G., Fiori, A., et al. (2019). Twenty-three unsolved problems in hydrology (UPH)—A community perspective. *Hydrological Sciences Journal*, 64(10), 1141–1158. <https://doi.org/10.1080/02626667.2019.1620507>
- Bonan, G. B. (1996). *A Land Surface Model (LSM Version 1.0) for ecological, hydrological, and atmospheric studies: Technical description and user's guide* (No. NCAR/TN-417+STR). University Corporation for Atmospheric Research. <https://doi.org/10.5065/D6DF6P5X>
- Bonan, G. B. (2015). Ecological climatology: Concepts and applications.
- Bouaziz, L. J. E., Steele-Dunne, S. C., Schellekens, J., Weerts, A. H., Stam, J., Sprokkereef, E., et al. (2020). Improved understanding of the link between catchment-scale vegetation accessible storage and satellite-derived Soil Water Index. *Water Resources Research*, 56(3), e2019WR026365. <https://doi.org/10.1029/2019wr026365>
- Braden, H. (1985). Ein energiehaushalts-und verdunstungsmodell für wasser und stoffhaushaltsuntersuchungen landwirtschaftlich genutzter einzugsgebiete. *Mitteilungen Deutsche Bodenkundliche Gesellschaft*, 42(S), 294–299.
- Brocca, L., Moramarco, T., Melone, F., Wagner, W., Hasenauer, S., & Hahn, S. (2011). Assimilation of surface-and root-zone ASCAT soil moisture products into rainfall-runoff modeling. *IEEE Transactions on Geoscience and Remote Sensing*, 50(7), 2542–2555. <https://doi.org/10.1109/tgrs.2011.2177468>
- Brunner, G. W. (2016). *HEC-RAS River Analysis System: Hydraulic reference manual, Version 5.0* (p. 547). US Army Corps of Engineers—Hydrologic Engineering Center.
- Buttinger-Kreuzhuber, A., Konev, A., Horváth, Z., Cornel, D., Schwerdorf, I., Blöschl, G., & Waser, J. (2022). An integrated GPU-accelerated modeling framework for high-resolution simulations of rural and urban flash floods. *Environmental Modelling & Software*, 156(July), 105480. <https://doi.org/10.1016/j.envsoft.2022.105480>
- Cea, L., Álvarez, M., & Puertas, J. (2022). Estimation of flood-exposed population in data-scarce regions combining satellite imagery and high resolution hydrological-hydraulic modelling: A case study in the Licungo basin (Mozambique). *Journal of Hydrology: Regional Studies*, 44, 101247. <https://doi.org/10.1016/j.ejrh.2022.101247>
- Cea, L., Álvarez, M., & Puertas, J. (2024). Using integrated hydrological-hydraulic modelling and global data sources to analyse the February 2023 floods in the Umbeluzi Catchment (Mozambique). *Natural Hazards and Earth System Sciences*, 24(1), 225–243. <https://doi.org/10.5194/nhess-24-225-2024>
- Cea, L., & Bladé, E. (2015). A simple and efficient unstructured finite volume scheme for solving the shallow water equations in overland flow applications. *Water Resources Research*, 51(7), 5464–5486. <https://doi.org/10.1002/2014wr016547>
- Cea, L., Garrido, M., & Puertas, J. (2010). Experimental validation of two-dimensional depth-averaged models for forecasting rainfall-runoff from precipitation data in urban areas. *Journal of Hydrology*, 382(1–4), 88–102. <https://doi.org/10.1016/j.jhydrol.2009.12.020>
- Cea, L., Garrido, M., Puertas, J., Jácome, A., Del Río, H., & Suárez, J. (2010). Overland flow computations in urban and industrial catchments from direct precipitation data using a two-dimensional shallow water model. *Water Science and Technology*, 62(9), 1998–2008. <https://doi.org/10.2166/wst.2010.746>
- Cea, L., Legout, C., Darboux, F., Esteves, M., & Nord, G. (2014). Experimental validation of a 2D overland flow model using high resolution water depth and velocity data. *Journal of Hydrology*, 513, 142–153. <https://doi.org/10.1016/j.jhydrol.2014.03.052>
- Chow, V. T. (1959). *Open channel hydraulics*. McGraw-Hill.
- Cimini, D., Romano, F., Ricciardelli, E., Di Paola, F., Viggiano, M., Marzano, F. S., et al. (2013). Validation of satellite OPEMW precipitation product with ground-based weather radar and rain gauge networks. *Atmospheric Measurement Techniques*, 6(11), 3181–3196. <https://doi.org/10.5194/amt-6-3181-2013>

- Clark, M. P., Nijssen, B., Lundquist, J. D., Kavetski, D., Rupp, D. E., Woods, R. A., et al. (2015). A unified approach for process-based hydrologic modeling: 1. Modeling concept. *Water Resources Research*, 51(4), 2498–2514. <https://doi.org/10.1002/2015wr017198>
- Coscarelli, R., Caloiero, T., Minervino, I., & Sorriso-Valvo, M. (2016). Sensitivity to desertification of a high productivity area in Southern Italy. *Journal of Maps*, 12(3), 573–581. <https://doi.org/10.1080/17445647.2015.1054904>
- Costabile, P., Cea, L., Barbaro, G., Costanzo, C., Llena, M., & Vericat, D. (2024). Evaluation of 2D hydrodynamic-based rainfall/runoff modelling for soil erosion assessment at a seasonal scale. *Journal of Hydrology*, 632, 130778. <https://doi.org/10.1016/j.jhydrol.2024.130778>
- Costabile, P., & Costanzo, C. (2021). A 2D-SWEs framework for efficient catchment-scale simulations: Hydrodynamic scaling properties of river networks and implications for non-uniform grids generation. *Journal of Hydrology*, 599(February), 126306. <https://doi.org/10.1016/j.jhydrol.2021.126306>
- Costabile, P., Costanzo, C., De Bartolo, S., Gangi, F., Macchione, F., & Tomasicchio, G. R. (2019). Hydraulic characterization of river networks based on flow patterns simulated by 2-D shallow water modeling: Scaling properties, multifractal interpretation, and perspectives for channel heads detection. *Water Resources Research*, 55(9), 7717–7752. <https://doi.org/10.1029/2018WR024083>
- Costabile, P., Costanzo, C., De Lorenzo, G., & Macchione, F. (2020). Is local flood hazard assessment in urban areas significantly influenced by the physical complexity of the hydrodynamic inundation model? *Journal of Hydrology*, 580(September 2019), 124231. <https://doi.org/10.1016/j.jhydrol.2019.124231>
- Costabile, P., Costanzo, C., & Macchione, F. (2013). A storm event watershed model for surface runoff based on 2D fully dynamic wave equations. *Hydrological Processes*, 27(4), 554–569. <https://doi.org/10.1002/hyp.9237>
- Dal Molin, M., Schirmer, M., Zappa, M., & Fencica, F. (2020). Understanding dominant controls on streamflow spatial variability to set up a semi-distributed hydrological model: The case study of the Thur catchment. *Hydrology and Earth System Sciences*, 24(3), 1319–1345. <https://doi.org/10.5194/hess-24-1319-2020>
- Dearhoff, J. W. (1978). Efficient prediction of ground surface temperature and moisture, with inclusion of a layer of vegetation. *Journal of Geophysical Research*, 83(C4), 1889–1903. <https://doi.org/10.1029/jc083ic04p01889>
- de Brogniez, D., Ballabio, C., Stevens, A., Jones, R. J. A., Montanarella, L., & van Wesemael, B. (2015). A map of the topsoil organic carbon content of Europe generated by a generalized additive model. *European Journal of Soil Science*, 66(1), 121–134. <https://doi.org/10.1111/ejss.12193>
- De Smedt, F., Yongbo, L., & Gebremeskel, S. (2000). Hydrologic modelling on a catchment scale using GIS and remote sensed land use information. *WIT Transactions on Ecology and the Environment*, 45, 1–10.
- Di Baldassarre, G., Schumann, G., & Bates, P. D. (2009). A technique for the calibration of hydraulic models using uncertain satellite observations of flood extent. *Journal of Hydrology*, 367(3–4), 276–282. <https://doi.org/10.1016/j.jhydrol.2009.01.020>
- Dickinson, R. E. (1984). Modeling evapotranspiration for three-dimensional global climate models. In *Climate processes and climate sensitivity* (Vol. 29, pp. 58–72). <https://doi.org/10.1029/gm029p0058>
- Dunne, T. (1991). Stochastic aspects of the relations between climate, hydrology and landform evolution. *Transactions - Japanese Geomorphological Union*, 12(1), 1–24.
- Dunne, T., & Leopold, L. B. (1978). *Water in environmental planning*. Macmillan.
- Eagleson, P. S. (1978). Climate, soil, and vegetation: 5. A derived distribution of storm surface runoff. *Water Resources Research*, 14(5), 741–748. <https://doi.org/10.1029/wr014i005p00741>
- Eagleson, P. S. (1982). Ecological optimality in water-limited natural soil-vegetation systems: 1. Theory and hypothesis. *Water Resources Research*, 18(2), 325–340. <https://doi.org/10.1029/wr018i002p00325>
- Engman, E. T. (1986). Roughness coefficients for routing surface runoff. *Journal of Irrigation and Drainage Engineering*, 112(1), 39–53. [https://doi.org/10.1061/\(asce\)0733-9437\(1986\)112:1\(39\)](https://doi.org/10.1061/(asce)0733-9437(1986)112:1(39))
- Famiglietti, J. S., & Wood, E. F. (1994). Multiscale modeling of spatially variable water and energy balance processes. *Water Resources Research*, 30(11), 3061–3078. <https://doi.org/10.1029/94wr01498>
- Fencica, F., Kavetski, D., Savenije, H. H. G., Clark, M. P., Schoups, G., Pfister, L., & Freer, J. (2014). Catchment properties, function, and conceptual model representation: Is there a correspondence? *Hydrological Processes*, 28(4), 2451–2467. <https://doi.org/10.1002/hyp.9726>
- Fencica, F., Kavetski, D., Savenije, H. H. G., & Pfister, L. (2016). From spatially variable streamflow to distributed hydrological models: Analysis of key modeling decisions. *Water Resources Research*, 52(2), 954–989. <https://doi.org/10.1002/2015wr017398>
- Fencica, F., & McDonnell, J. J. (2022). Modeling streamflow variability at the regional scale: (1) Perceptual model development through signature analysis. *Journal of Hydrology*, 605, 127287. <https://doi.org/10.1016/j.jhydrol.2021.127287>
- Fencica, F., McDonnell, J. J., & Savenije, H. H. G. (2008). Learning from model improvement: On the contribution of complementary data to process understanding. *Water Resources Research*, 44(6), W06419. <https://doi.org/10.1029/2007wr006386>
- Fencica, F., Meißner, D., & McDonnell, J. J. (2022). Modeling streamflow variability at the regional scale: (2) Development of a bespoke distributed conceptual model. *Journal of Hydrology*, 605, 127286. <https://doi.org/10.1016/j.jhydrol.2021.127286>
- Fiorentino, M., Manfreda, S., & Iacobellis, V. (2007). Peak runoff contributing area as hydrological signature of the probability distribution of floods. *Advances in Water Resources*, 30(10), 2123–2134. <https://doi.org/10.1016/j.advwatres.2006.11.017>
- Fraga, I., Cea, L., & Puertas, J. (2019). Effect of rainfall uncertainty on the performance of physically based rainfall–runoff models. *Hydrological Processes*, 33(1), 160–173. <https://doi.org/10.1002/hyp.13319>
- Freeze, R. A. (1974). Streamflow generation. *Reviews of Geophysics*, 12(4), 627–647. <https://doi.org/10.1029/rg012i004p00627>
- García-Feal, O., González-Cao, J., Gómez-Gesteira, M., Cea, L., Domínguez, J. M., & Formella, A. (2018). An accelerated tool for flood modelling based on Iber. *Water (Switzerland)*, 10(10), 1–23. <https://doi.org/10.3390/w10101459>
- Gigante, V., Iacobellis, V., Manfreda, S., Milella, P., & Portoghesi, I. (2009). Influences of leaf area index estimations on water balance modeling in a Mediterranean semi-arid basin. *Natural Hazards and Earth System Sciences*, 9(3), 979–991. <https://doi.org/10.5194/nhess-9-979-2009>
- Godara, N., Bruland, O., & Alfredsen, K. (2023). Simulation of flash flood peaks in a small and steep catchment using rain-on-grid technique. *Journal of Flood Risk Management*, 16(3), 1–14. <https://doi.org/10.1111/jfr3.12898>
- Goudenhoofd, E., & Delobbe, L. (2009). Evaluation of radar-gauge merging methods for quantitative precipitation estimates. *Hydrology and Earth System Sciences*, 13(2), 195–203. <https://doi.org/10.5194/hess-13-195-2009>
- Grillakis, M. G., Koutroulis, A. G., Komma, J., Tsanis, I. K., Wagner, W., & Blöschl, G. (2016). Initial soil moisture effects on flash flood generation—A comparison between basins of contrasting hydro-climatic conditions. *Journal of Hydrology*, 541, 206–217. <https://doi.org/10.1016/j.jhydrol.2016.03.007>
- Guerrini, A., Lavagnini, A., & Vivona, F. (1977). *L'insolazione sull'Italia*. Istituto Di Fisica Dell'Atmosfera.
- Gupta, H. V., Kling, H., Yilmaz, K. K., & Martinez, G. F. (2009). Decomposition of the mean squared error and NSE performance criteria: Implications for improving hydrological modelling. *Journal of Hydrology*, 377(1–2), 80–91. <https://doi.org/10.1016/j.jhydrol.2009.08.003>



- Hall, J. (2015). Direct rainfall flood modelling: The good, the bad and the ugly. *Australian Journal of Water Resources*, 19(1), 74–85. <https://doi.org/10.7158/13241583.2015.11465458>
- Hawkins, R. H., Ward, T. J., Woodward, D. E., & Van Mullem, J. A. (2008). Curve number hydrology: State of the practice.
- Herrera, P. A., Marazuela, M. A., & Hofmann, T. (2022). Parameter estimation and uncertainty analysis in hydrological modeling. *Wiley Interdisciplinary Reviews: Water*, 9(1), e1569. <https://doi.org/10.1002/wat2.1569>
- Hiemstra, P. H., Pebesma, E. J., Twenhöfel, C. J. W., & Heuvelink, G. B. M. (2009). Real-time automatic interpolation of ambient gamma dose rates from the Dutch radioactivity monitoring network. *Computers & Geosciences*, 35(8), 1711–1721. <https://doi.org/10.1016/j.cageo.2008.10.011>
- Horton, R. E. (1933). The role of infiltration in the hydrologic cycle. *Eos, Transactions American Geophysical Union*, 14(1), 446–460.
- Horton, R. E. (1941). An approach toward a physical interpretation of infiltration-capacity 1. *Soil Science Society of America Journal*, 5(C), 399–417. <https://doi.org/10.2136/sssaj1941.036159950005000c0075x>
- Iacobellis, V., Gioia, A., Milella, P., Satalino, G., Balenzano, A., & Mattia, F. (2013). Inter-comparison of hydrological model simulations with time series of SAR-derived soil moisture maps. *European Journal of Remote Sensing*, 46(1), 739–757. <https://doi.org/10.5721/EuJRS20134644>
- Jaafar, H. H., Ahmad, F. A., & El Beyrouthy, N. (2019). GCN250, new global gridded curve numbers for hydrologic modeling and design. *Scientific Data*, 6(1), 145. <https://doi.org/10.1038/s41597-019-0155-x>
- Jewell, S. A., & Gaussiat, N. (2015). An assessment of kriging-based rain-gauge-radar merging techniques. *Quarterly Journal of the Royal Meteorological Society*, 141(691), 2300–2313. <https://doi.org/10.1002/qj.2522>
- Kastens, K. A., Manduca, C. A., Cervato, C., Frodeman, R., Goodwin, C., Liben, L. S., et al. (2009). How geoscientists think and learn. *Eos, Transactions American Geophysical Union*, 90(31), 265–266. <https://doi.org/10.1029/2009EO310001>
- Kim, K. B., Kwon, H.-H., & Han, D. (2018). Exploration of warm-up period in conceptual hydrological modelling. *Journal of Hydrology*, 556, 194–210. <https://doi.org/10.1016/j.jhydrol.2017.11.015>
- Kirchner, J. W. (2006). Getting the right answers for the right reasons: Linking measurements, analyses, and models to advance the science of hydrology. *Water Resources Research*, 42(3), W03504. <https://doi.org/10.1029/2005wr004362>
- Kirkby, M. J. (1975). Hydrograph modeling strategies. In *Process in physical and human geography* (pp. 69–90).
- Krause, P., Boyle, D. P., & Båse, F. (2005). Comparison of different efficiency criteria for hydrological model assessment. *Advances in Geosciences*, 5, 89–97. <https://doi.org/10.5194/adgeo-5-89-2005>
- Lacasta, A., Morales-Hernández, M., Murillo, J., & García-Navarro, P. (2015). GPU implementation of the 2D shallow water equations for the simulation of rainfall/runoff events. *Environmental Earth Sciences*, 74(11), 7295–7305. <https://doi.org/10.1007/s12665-015-4215-z>
- Larcher, W. (1975). Physiological plant ecology.
- Linsley, R. K., Jr., Kohler, M. A., & Paulhus, J. L. H. (1975). Hydrology for engineers.
- Liu, Y. B., & De Smedt, F. (2004). *WetSpa extension, A GIS-based hydrological model for flood prediction and water management, documentation and user manual*. Department of Hydrology and Hydraulic Engineering, Vrije Universiteit Brussel.
- Macchione, F., Costabile, P., Costanzo, C., & De Lorenzo, G. (2019). Extracting quantitative data from non-conventional information for the hydraulic reconstruction of past urban flood events. A case study. *Journal of Hydrology*, 576(February), 443–465. <https://doi.org/10.1016/j.jhydrol.2019.06.031>
- Madsen, H. (2000). Automatic calibration of a conceptual rainfall–runoff model using multiple objectives. *Journal of Hydrology*, 235(3–4), 276–288. [https://doi.org/10.1016/S0022-1694\(00\)00279-1](https://doi.org/10.1016/S0022-1694(00)00279-1)
- Manabe, S. (1969). The atmospheric circulation and hydrology of the Earth's surface. *Monthly Weather Review*, 97(11), 739–774. [https://doi.org/10.1175/1520-0493\(1969\)097<0739:catoc>2.3.co;2](https://doi.org/10.1175/1520-0493(1969)097<0739:catoc>2.3.co;2)
- Manfreda, S., Fiorentino, M., & Iacobellis, V. (2005). DREAM: A distributed model for runoff, evapotranspiration, and antecedent soil moisture simulation. *Advances in Geosciences*, 2, 31–39. <https://doi.org/10.5194/adgeo-2-31-2005>
- Manfreda, S., Lacava, T., Onorati, B., Pergola, N., Di Leo, M., Margiotta, M. R., & Tramutoli, V. (2011). On the use of AMSU-based products for the description of soil water content at basin scale. *Hydrology and Earth System Sciences*, 15(9), 2839–2852. <https://doi.org/10.5194/hess-15-2839-2011>
- Masafu, C., & Williams, R. (2024). Satellite video remote sensing for flood model validation. *Water Resources Research*, 60(1), e2023WR034545. <https://doi.org/10.1029/2023WR034545>
- Massari, C., Brocca, L., Barbetta, S., Papathanasiou, C., Mimikou, M., & Moramarco, T. (2014). Using globally available soil moisture indicators for flood modelling in Mediterranean catchments. *Hydrology and Earth System Sciences*, 18(2), 839–853. <https://doi.org/10.5194/hess-18-839-2014>
- McDonnell, J. J. (1990). A rationale for old water discharge through macropores in a steep, humid catchment. *Water Resources Research*, 26(11), 2821–2832. <https://doi.org/10.1029/wr026i011p02821>
- McDonnell, J. J., Sivapalan, M., Vaché, K., Dunn, S., Grant, G., Haggerty, R., et al. (2007). Moving beyond heterogeneity and process complexity: A new vision for watershed hydrology. *Water Resources Research*, 43(7), W07301. <https://doi.org/10.1029/2006wr005467>
- McMillan, H. (2022). A taxonomy of hydrological processes and watershed function. *Hydrological Processes*, 36(3), 1–7. <https://doi.org/10.1002/hyp.14537>
- Merz, B., & Thielen, A. H. (2005). Separating natural and epistemic uncertainty in flood frequency analysis. *Journal of Hydrology*, 309(1–4), 114–132. <https://doi.org/10.1016/j.jhydrol.2004.11.015>
- Milella, P., Bisantino, T., Gentile, F., Iacobellis, V., & Trisorio Liuzzi, G. (2012). Diagnostic analysis of distributed input and parameter datasets in Mediterranean basin streamflow modeling. *Journal of Hydrology*, 472–473, 262–276. <https://doi.org/10.1016/j.jhydrol.2012.09.039>
- Ming, X., Liang, Q., Xia, X., Li, D., & Fowler, H. J. (2020). Real-time flood forecasting based on a high-performance 2-D hydrodynamic model and numerical weather predictions. *Water Resources Research*, 56(7), e2019WR025583. <https://doi.org/10.1029/2019wr025583>
- Mockus, V. (1964). *National engineering handbook* (Vol. 4). US Soil Conservation Service.
- Montalvo, C., Reyes-Silva, J. D., Sañudo, E., Cea, L., & Puertas, J. (2024). Urban pluvial flood modelling in the absence of sewer drainage network data: A physics-based approach. *Journal of Hydrology*, 634, 131043. <https://doi.org/10.1016/j.jhydrol.2024.131043>
- Muñoz-Sabater, J., Dutra, E., Agustí-Panareda, A., Albergel, C., Arduini, G., Balsamo, G., et al. (2021). ERA5-Land: A state-of-the-art global reanalysis dataset for land applications. *Earth System Science Data*, 13(9), 4349–4383. <https://doi.org/10.5194/essd-13-4349-2021>
- Myneni, R., Knyazikhin, Y., & Park, T. (2021). MODIS/Terra+Aqua Leaf Area Index/FPAR 4-day L4 global 500m SIN grid V061 [Dataset]. *NASA EOSDIS Land Processes Distributed Active Archive Center*. <https://doi.org/10.5067/MODIS/MCD15A3H.061>
- Nanding, N., Rico-Ramirez, M. A., & Han, D. (2015). Comparison of different radar-raingauge rainfall merging techniques. *Journal of Hydroinformatics*, 17(3), 422–445. <https://doi.org/10.2166/hydro.2015.001>

- Nearing, G. S., Tian, Y., Gupta, H. V., Clark, M. P., Harrison, K. W., & Wejls, S. V. (2016). A philosophical basis for hydrological uncertainty. *Hydrological Sciences Journal*, *61*(9), 1666–1678. <https://doi.org/10.1080/02626667.2016.1183009>
- Nied, M., Schröter, K., Lüdtke, S., Nguyen, V. D., & Merz, B. (2017). What are the hydro-meteorological controls on flood characteristics? *Journal of Hydrology*, *545*, 310–326. <https://doi.org/10.1016/j.jhydrol.2016.12.003>
- USDA NRCS. (2004). *National engineering handbook: Part 630—Hydrology* (pp. 11–15). USDA Soil Conservation Service.
- Orth, R., Staudinger, M., Seneviratne, S. I., Seibert, J., & Zappa, M. (2015). Does model performance improve with complexity? A case study with three hydrological models. *Journal of Hydrology*, *523*, 147–159. <https://doi.org/10.1016/j.jhydrol.2015.01.044>
- Paniconi, C., & Putti, M. (2015). Physically based modeling in catchment hydrology at 50: Survey and outlook. *Water Resources Research*, *51*(9), 7090–7129. <https://doi.org/10.1002/2015wr017780>
- Perrin, C., Michel, C., & Andréassian, V. (2001). Does a large number of parameters enhance model performance? Comparative assessment of common catchment model structures on 429 catchments. *Journal of Hydrology*, *242*(3–4), 275–301. [https://doi.org/10.1016/s0022-1694\(00\)00393-0](https://doi.org/10.1016/s0022-1694(00)00393-0)
- Pfannerstill, M., Guse, B., & Fohrer, N. (2014). Smart low flow signature metrics for an improved overall performance evaluation of hydrological models. *Journal of Hydrology*, *510*, 447–458. <https://doi.org/10.1016/j.jhydrol.2013.12.044>
- Ponce, V. M., & Hawkins, R. H. (1996). Runoff curve number: Has it reached maturity? *Journal of Hydrologic Engineering*, *1*(1), 11–19. [https://doi.org/10.1061/\(asce\)1084-0699\(1996\)1:1\(11\)](https://doi.org/10.1061/(asce)1084-0699(1996)1:1(11))
- Prescott, J. A. (1940). Evaporation from a water surface in relation to solar radiation. *Transactions of the Royal Society of South Australia*, *46*, 114–118.
- Rawls, W. J., & Brakensiek, D. L. (1985). Prediction of soil water properties for hydrologic modeling. In *Watershed management in the eighties* (pp. 293–299).
- Rawls, W. J., Brakensiek, D. L., & Saxton, K. E. (1982). Estimation of soil water properties. *Transactions of the ASAE*, *25*(5), 1316–1320. <https://doi.org/10.13031/2013.33720>
- Rehman, H. U., Zollinger, M. W., & Collings, G. B. (2003). Hydrological vs hydraulic routing possibilities with two-dimensional hydraulic modelling. In *28th International Hydrology and Water Resources Symposium: About Water; Symposium Proceedings* (pp. 3–31).
- Rigon, R., Formetta, G., Bancheri, M., Tubini, N., D'Amato, C., David, O., & Massari, C. (2022). HESS Opinions: Participatory Digital Earth Twin Hydrology systems (DARTHS) for everyone: A blueprint for hydrologists. *Hydrology and Earth System Sciences Discussions*, *2022*, 1–38. <https://doi.org/10.5194/hess-2021-644>
- Rivieccio, R., Di Bene, C., Paolanti, M., Marchetti, M., & Napoli, R. (2020). Soil rooting depth of Italy. *Journal of Maps*, *16*(2), 36–42. <https://doi.org/10.1080/17445647.2019.1690595>
- Rossi, F., Fiorentino, M., & Versace, P. (1984). Two-component extreme value distribution for flood frequency analysis. *Water Resources Research*, *20*(7), 847–856. <https://doi.org/10.1029/wr020i007p00847>
- Sañudo, E., Cea, L., Puertas, J., Naves, J., & Anta, J. (2024). Large-scale physical facility and experimental dataset for the validation of urban drainage models. *Hydrological Processes*, *38*(1), e15068. <https://doi.org/10.1002/hyp.15068>
- Savenije, H. H. G. (2009). HESS Opinions “The art of hydrology”. *Hydrology and Earth System Sciences*, *13*(2), 157–161. <https://doi.org/10.5194/hess-13-157-2009>
- Savenije, H. H. G. (2010). HESS Opinions “Topography driven conceptual modelling (FLEX-Topo)”. *Hydrology and Earth System Sciences*, *14*(12), 2681–2692. <https://doi.org/10.5194/hess-14-2681-2010>
- Saxton, K. E., & Rawls, W. J. (2006). Soil water characteristic estimates by texture and organic matter for hydrologic solutions. *Soil Science Society of America Journal*, *70*(5), 1569–1578. <https://doi.org/10.2136/sssaj2005.0117>
- Schumann, G. J.-P., & Moller, D. K. (2015). Microwave remote sensing of flood inundation. *Physics and Chemistry of the Earth, Parts A/B/C*, *83*, 84–95. <https://doi.org/10.1016/j.pce.2015.05.002>
- Silveira, L., Charbonnier, F., & Genta, J. L. (2000). The antecedent soil moisture condition of the curve number procedure. *Hydrological Sciences Journal*, *45*(1), 3–12. <https://doi.org/10.1080/02626660009492302>
- Sivapalan, M. (2003). Process complexity at hillslope scale, process simplicity at watershed scale: Is there a connection? *EGS-AGU-EUG Joint Assembly*, 7973.
- Staudinger, M., Stoelzle, M., Cochand, F., Seibert, J., Weiler, M., & Hunkeler, D. (2019). Your work is my boundary condition!: Challenges and approaches for a closer collaboration between hydrologists and hydrogeologists. *Journal of Hydrology*, *571*(February), 235–243. <https://doi.org/10.1016/j.jhydrol.2019.01.058>
- Tamagnone, P., Cea, L., Comino, E., & Rosso, M. (2020). Rainwater harvesting techniques to face water scarcity in African drylands: Hydrological efficiency assessment. *Water*, *12*(9), 2646. <https://doi.org/10.3390/w12092646>
- Tamagnone, P., Comino, E., & Rosso, M. (2020). Rainwater harvesting techniques as an adaptation strategy for flood mitigation. *Journal of Hydrology*, *586*(December 2019), 124880. <https://doi.org/10.1016/j.jhydrol.2020.124880>
- Tartakovsky, D. M. (2007). Probabilistic risk analysis in subsurface hydrology. *Geophysical Research Letters*, *34*(5), L05404. <https://doi.org/10.1029/2007gl029245>
- Tedela, N. H., McCutcheon, S. C., Rasmussen, T. C., Hawkins, R. H., Swank, W. T., Campbell, J. L., et al. (2012). Runoff curve numbers for 10 small forested watersheds in the mountains of the eastern United States. *Journal of Hydrologic Engineering*, *17*(11), 1188–1198. [https://doi.org/10.1061/\(asce\)he.1943-5584.0000436](https://doi.org/10.1061/(asce)he.1943-5584.0000436)
- Uber, M., Nord, G., Legout, C., & Cea, L. (2021). How do modeling choices and erosion zone locations impact the representation of connectivity and the dynamics of suspended sediments in a multi-source soil erosion model? *Earth Surface Dynamics*, *9*(1), 123–144. <https://doi.org/10.5194/esurf-9-123-2021>
- van Esse, W. R., Perrin, C., Booij, M. J., Augustijn, D. C. M., Fenicia, F., Kavetski, D., & Lobligeois, F. (2013). The influence of conceptual model structure on model performance: A comparative study for 237 French catchments. *Hydrology and Earth System Sciences*, *17*(10), 4227–4239. <https://doi.org/10.5194/hess-17-4227-2013>
- Viessman, W., Lewis, G. L., Knapp, J. W., & Harbaugh, T. E. (1989). Introduction to hydrology.
- Viglione, A., Claps, P., & Laio, F. (2007). Mean annual runoff estimation in North-Western Italy. In *Water Resources Assessment and Management under water scarcity scenarios* (Vol. 97), 122.
- Von-Hoyningen-Huene, J. (1983). Die Interzeption des Niederschlags in landwirtschaftlichen Pflanzenbeständen.
- Wagner, W., Lemoine, G., & Rott, H. (1999). A method for estimating soil moisture from ERS Scatterometer and soil data. *Remote Sensing of Environment*, *70*(2), 191–207. [https://doi.org/10.1016/S0034-4257\(99\)00036-X](https://doi.org/10.1016/S0034-4257(99)00036-X)
- Walega, A., Amatya, D. M., Caldwell, P., Marion, D., & Panda, S. (2020). Assessment of storm direct runoff and peak flow rates using improved SCS-CN models for selected forested watersheds in the Southeastern United States. *Journal of Hydrology: Regional Studies*, *27*, 100645. <https://doi.org/10.1016/j.ejrh.2019.100645>

- Weiler, M., McDonnell, J. J., Tromp-van Meerveld, I., & Uchida, T. (2006). Subsurface stormflow. In *Encyclopedia of hydrological sciences*.
- Xia, X., Liang, Q., & Ming, X. (2019). A full-scale fluvial flood modelling framework based on a high-performance integrated hydrodynamic modelling system (HiPIMS). *Advances in Water Resources*, *132*(March), 103392. <https://doi.org/10.1016/j.advwatres.2019.103392>
- Zhang, H., Huang, G. H., Wang, D., & Zhang, X. (2011). Multi-period calibration of a semi-distributed hydrological model based on hydro-climatic clustering. *Advances in Water Resources*, *34*(10), 1292–1303. <https://doi.org/10.1016/j.advwatres.2011.06.005>